

Article

The Esquinzo Ultra-Alkaline Rock Suite of Fuerteventura Basal Complex (Canary Islands): Evidence for Origin of Carbonatites by Fractional Crystallization

Ramón Casillas ^{1,*}, Agustina Ahijado ^{1,†}, Géza Nagy ^{2,†}, Attila Demény ^{2,†} and Carlos Fernández ^{3,†} 

¹ Departamento de Biología Animal, Edafología y Geología, Universidad de La Laguna, P.O. Box 456, 38200 La Laguna, Spain; aahijado@ull.edu.es

² Institute for Geological and Geochemical Research, Research Center for Astronomy and Earth Sciences, Hungarian Academy for Sciences, HUN-REN, Budaörsi út 45, 1112 Budapest, Hungary; nagygeza41@t-online.hu (G.N.)

³ Departamento de Geodinámica, Estratigrafía y Paleontología, Facultad de Ciencias Geológicas, Universidad Complutense de Madrid, C. de José Antonio Novais, 12, 28040 Madrid, Spain; cafern08@ucm.es

* Correspondence: rcasilla@ull.edu.es; Tel.: +34-922845268

† These authors contributed equally to this work.

Abstract: The origin of the carbonatites that appear on Earth is one of the most controversial current topics in the petrogenesis of igneous rocks. Situated in the northern sector of the Basal Complex of Fuerteventura (Canary Islands), the Miocene Esquinzo ultra-alkaline plutonic rock complex is composed of pyroxenites, melteigites-ijolites-urtites, malignites-nepheline syenites, carbonatites, silicocarbonatites, nephelinites and nepheline phonolites. This work tries to establish the genesis of this massif of ultra-alkaline rocks with associated carbonatites from Fuerteventura (which are very rare in the oceans). The geochemical characteristics of these rocks and the minerals that are included in them have allowed us to establish their origin. This complex was generated by three successive magmatic events associated with differentiation of melanephelinite magmas emplaced in the oceanic crust. Silicocarbonatite and calciocarbonatite (sövites) dykes are related to the first magmatic event and were formed by fractional crystallization of H₂O- and CO₂-rich ijolite magmas. The melanephelinite magmas that formed these plutonic ultra-alkaline rocks were apparently generated as partial melts of asthenospheric mantle, which assimilated enriched lithospheric mantle material as they ascended. The upwelling of this large body of anomalous asthenospheric Miocene material exceeded the deformation associated with plate motions and led to an oceanic rifting event in Fuerteventura.

Keywords: Fuerteventura; carbonatite; fractional crystallization; oceanic island; melanephelinite



Citation: Casillas, R.; Ahijado, A.; Nagy, G.; Demény, A.; Fernández, C. The Esquinzo Ultra-Alkaline Rock Suite of Fuerteventura Basal Complex (Canary Islands): Evidence for Origin of Carbonatites by Fractional Crystallization. *Minerals* **2024**, *14*, 295. <https://doi.org/10.3390/min14030295>

Academic Editors: Federica Zaccarini, Enrique Merino Martínez, David Orejana García and Helena Sant'Ovaia

Received: 4 December 2023

Revised: 23 February 2024

Accepted: 27 February 2024

Published: 11 March 2024



Copyright: © 2024 by the authors. Licensee MDPI, Basel, Switzerland. This article is an open access article distributed under the terms and conditions of the Creative Commons Attribution (CC BY) license (<https://creativecommons.org/licenses/by/4.0/>).

1. Introduction

The scarcity of carbonatite outcrops in oceanic islands (i.e., only found in the Canary and Cape Verde Islands) makes these occurrences especially valuable for investigating carbonatite-generating processes [1–3]. Their scarcity contrasts with the greater abundance of undersaturated ultra-alkaline rocks in oceanic environments.

Carbonatites often occur in close spatial association with undersaturated alkaline igneous rocks with compositions varying between pyroxenites, nephelinites and/or ijolites, and more evolved nepheline syenites [4,5]. Le Bas [4] discussed the occurrence of two main nephelinite types: melanephelinites (pyroxene nephelinites) (Group I, olivine-poor nephelinites) and olivine-rich nephelinites (Group II). The former type is associated with ijolite-nepheline syenites, and frequently carbonatites, in ultra-alkaline plutonic complexes. The second type, olivine nephelinites, shows no relationship with these plutonic complexes. The author explained this difference in relation with olivine and pyroxene fractional crystallization processes of an olivine-rich nephelinite magma in crustal levels. This magma would fractionate to phonolite and a wide suite of plutonic ultra-alkaline rocks (alkali pyroxenites,

ijolites, nepheline syenites and carbonatites). In contrast, olivine-rich nephelinites could cross the crust without magmatic pausing.

The petrogenetic link between carbonatite and alkaline silicate rocks, both of mantle origin, is still discussed. Three petrogenetic processes have been proposed, all being related to the formation of a primary carbonate-rich melt derived from a carbonated mantle: (1) the low-degree partial melting of a carbonated mantle source [6–8], (2) immiscible separation from a CO₂-rich alkaline silicate melt [9–15], and (3) the late-stage result of fractional crystallization of a carbonated alkaline silicate melt [8,13,16,17].

In Fuerteventura, one of the easternmost islands of the Canary Archipelago, a complex group of ultra-alkaline rocks occurs as part of the ‘Basal Complex’ [18]. This unit comprises part of the Mesozoic oceanic crust, a series of submarine volcanic rocks (Submarine Volcanic Group, S.V.G., and Transitional Volcanic Group, T.V.G.), the earliest stages of subaerial growth of the island (Subaerial Volcanic Group, S.V.SA.), several plutonic intrusions and a dense dyke swarm [18–31].

In the lowest part of the S.V.G., Gutiérrez et al. [25–27] described the occurrence of volcanogenic horizons containing abundant fragments of nephelinite, nepheline phonolite, melteigite-ijolite, alkali pyroxenite and nepheline syenite. These horizons were formed partly from erosion and destruction of plutonic and hypabyssal rocks that form the ultra-alkaline complexes, which are composed of mica- and amphibole-bearing pyroxenites, melteigites-ijolites-urtites, amphibole-bearing gabbros, nepheline syenites, nephelinites and carbonatites [26]. Three complexes are located from north to south in Esquinzo, Ajuy-Solapa and Punta del Peñón Blanco [22,32–36] (Figure S1). The younger intrusions of this series were emplaced contemporaneously with displacement along brittle and ductile extensional shear zones [37,38] that were active during the Miocene period around 25 Ma ago [28,35,39]. In the Miocene Esquinzo complex, deformation is less severe, and a greater variety of ultra-alkaline plutonic rocks (alkali pyroxenites, ijolites s.l., syenites and carbonatites) and related nephelinite dykes has been recognized [18–33].

The main objective of this study is to provide a detailed petrological study of the different lithologies in the Esquinzo ultra-alkaline complex. We discuss the possible genetic relationship between silicate ultra-alkaline rocks and associated carbonatites.

1.1. Geological Background

The geological history of Fuerteventura is the most complex and long-lasting one among the Canary Islands. Six main units can be distinguished (Figure S1). These are (from older to younger): (a) Mesozoic oceanic crust relicts; (b) the ultra-alkaline plutonic complexes; (c) the Initial Volcanic Ridge; (d) the Miocene shield volcanoes; (e) the Plio-Quaternary volcanic rocks; and (f) the Plio-Quaternary sediments [18,19,22,24,27–29,31,36,39–41]. In Figure S2, the most important relationships between the main Oligocene and Miocene formations of Fuerteventura are shown.

The Mesozoic oceanic crust, the ultra-alkaline plutonic complexes, the lower part of the Initial Volcanic Ridge (the Submarine Volcanic Group, the S.V.G.; the Transitional Volcanic Group, the T.V.G.; and the Subaerial Volcanic Group, S.A.V.G.), the plutonic bodies and the dyke swarms associated with the Initial Volcanic Ridge and with the Miocene Shield Volcanoes form a heterogeneous lithostratigraphic unit known as the Basal Complex [18,19,22].

The Mesozoic oceanic crust comprises tholeiitic N-type mid-ocean-ridge basalts of Early Jurassic age overlain by a thick sedimentary sequence from the Early Jurassic to Late Cretaceous age [24]. Resting unconformably on the Mesozoic oceanic crust is the S.V.G., which represents the period of submarine growth of Fuerteventura [20–22,25–27]. Overlapping the S.V.G. is the T.V.G., corresponding to the emergence of the island [25–27]. Plutonic activity prior to the S.V.G. formed ultra-alkaline rocks that outcrop along the western coast of the island.

During the Oligocene period or earlier, Fuerteventura was affected by a contractional phase that produced the uplift and inversion of the outcropping oceanic crust rocks [27,28].

The Miocene growth of the island began with the generation of a large volcanic ridge [28]. Associated with this Initial Volcanic Ridge, various plutons were formed, mainly of gabbros and pyroxenites, and an important dyke swarm was formed in the NE-SW direction. This initial volcanic ridge suffered significant gravitational landslides on its western flank. Behind these, and within the amphitheaters generated by these landslides, three large shield volcanoes were formed: the southern, central and northern edifices (Southern Volcanic complex, S.V.C; Central Volcanic complex, C.V.C.; and Northern Volcanic complex, N.V.C.; [41]; Figures S1 and S2). A series of plutonic rocks (pyroxenites, gabbros and syenites) and dyke swarms (basalts and trachybasalts) outcrop in the core of the northern and central edifices (e.g., Pájara Pluton) [22,23,42–44]. They represent the hypabyssal roots of successive growth episodes of the subaerial volcanic edifices [41]. An intense hydrothermal metamorphism of epidote-albite greenschist facies took place, probably as a result of the massive intrusion of dyke swarms [21,27,45]. Intrusion of plutons related to the Initial Volcanic Ridge and the Miocene shield volcanoes caused significant contact metamorphism in the neighboring rocks [43,45–50]. Three Miocene extensional deformation phases (M-D1, M-D2 and M-D3) are recognized in Fuerteventura [28].

A period of quiescence followed the Miocene subaerial volcanic activity, and the edifices were deeply eroded. Small basaltic volcanoes and associated lava fields resulted from renewed activity during the Pliocene period that continued to prehistoric times [18]. Littoral and shallow-water marine deposits, aeolian and alluvial complexes and paleosol deposits were generated in the Plio-Quaternary period [51].

1.2. Field Relations

The main outcrops of the Esquinzo ultra-alkaline complex are located in the ravines south of Montaña Blanca and in the cliffs along the western coast from Playa del Aguila to Playa de Tebeto (Figure 1). Other peripheral outcrops occur in Montaña de Los Frailes, north of Montaña Blanca (Figure 1). The Esquinzo ultra-alkaline complex is in faulted contact with oceanic crustal sedimentary rocks south of Playa de Tebeto (Figure 1). The relationships between the S.V.G., the T.V.G. and the ultra-alkaline rocks are not clear due to the absence of outcrops in this area.

The Esquinzo ultra-alkaline complex is surrounded by polymict breccias (debris-avalanche and debris-flow deposits), pyroclastics and ‘pahoehoe’ and ‘aa’ lava-flows of basaltic-trachybasaltic composition. Fúster et al. [18] and Barrera et al. [33] considered that these volcanic materials (pyroclastics and ‘pahoehoe’ and ‘aa’ lava-flows of basaltic-trachybasaltic composition) belong to the Submarine Volcanic Series that represents the host-rock of the ultra-alkaline intrusions. More recently, several studies [25–27] have shown the subaerial character of these volcanic rocks that belong to the early volcanic ridge [28].

In many locations, the basaltic-trachybasaltic subaerial rocks (pyroclastics and ‘pahoehoe’ lava-flows) lie unconformably on the ultra-alkaline complex (Figure 2a). These units are separated by a polygenetic breccia (up to 70 cm thick) composed of a clay-sandy matrix rich in iron oxides and heterogeneous plutonic and volcanic fragments (ferricrete) (Figure 2b). This breccia was first described by Fúster et al. [18], and it was previously interpreted by Barrera et al. [33] as a fluidized breccia formed by the action of late hydrothermal fluids related to the ultra-alkaline intrusions. This unconformity can be observed in many localities (Figure 3). It always dips westward and is parallel to the subaerial basaltic-trachybasaltic lava flows that overlie it. This orientation could be due to tilting related to regional uplift, coeval with the main dyke swarm intrusion, which affected the during the Early Miocene period [41] extensional deformation phase M-D1 (Figure S2, after [28]).

Both the ultra-alkaline plutonic intrusions and the subaerial volcanic materials of the Initial Volcanic Ridge were intruded and thermally metamorphosed by the ultramafic-mafic plutonic rocks of Montaña Blanca [18,33]. These plutons are equivalent in relative age and composition to the ultramafic intrusions in the Betancuria Massif (e.g., Pájara Pluton) that are probably related to the Initial Volcanic Ridge [22,31,39,41,43].

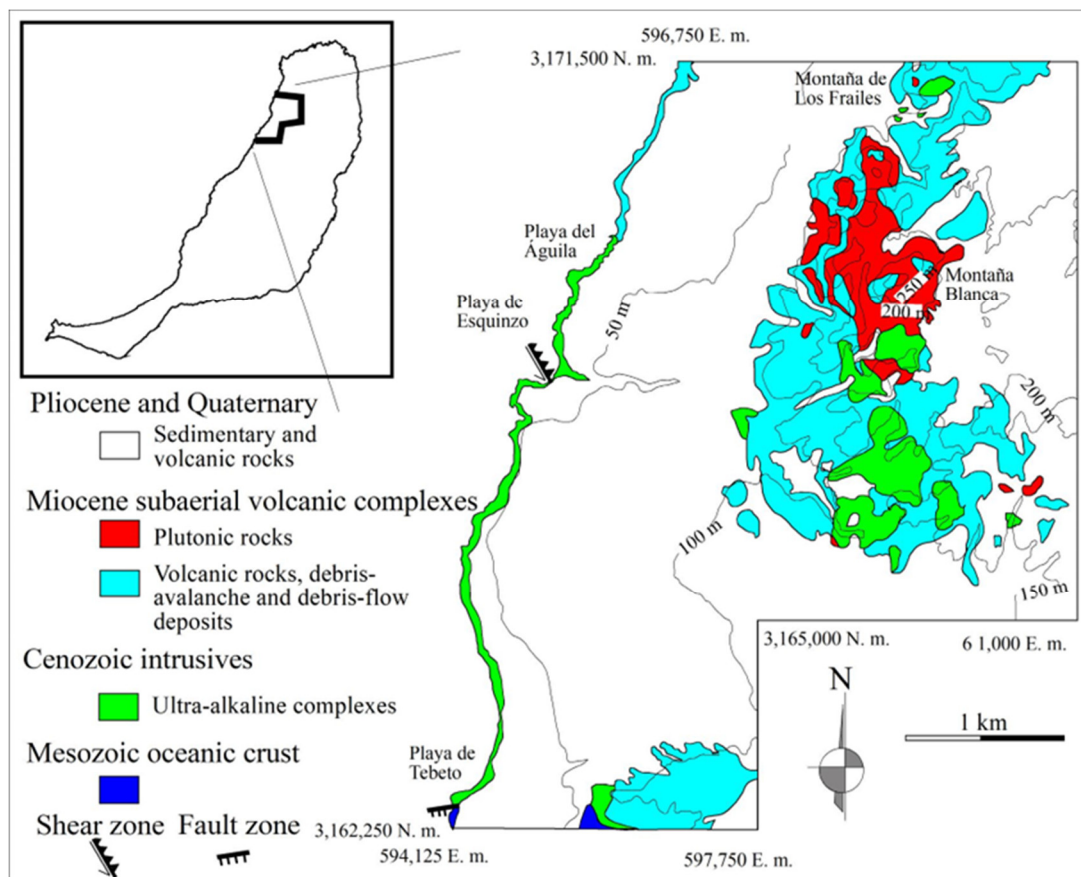


Figure 1. Geological map of the northern part of the Basal Complex of Fuerteventura. Modified after the 1:25,000 National Geological Map [52,53]. The inset shows the location of the mapped area on Fuerteventura Island.

The results of the intrusion of these magmas into their country rocks can be best observed from points I to III in Figure 3. A small gabbroic intrusion emplaced into ijolites and subaerial volcanic materials at point I has caused the formation of hornfels and spotted rocks with biotite porphyroblasts. At point II, the Montaña Blanca gabbros intruded, metamorphosed and brecciated their host rocks (subaerial volcanic materials, ijolites and syenites). Montaña Blanca gabbro also produced anatexite-like feldspathic veins within alkali pyroxenites and basaltic dykes, as observed at point III.

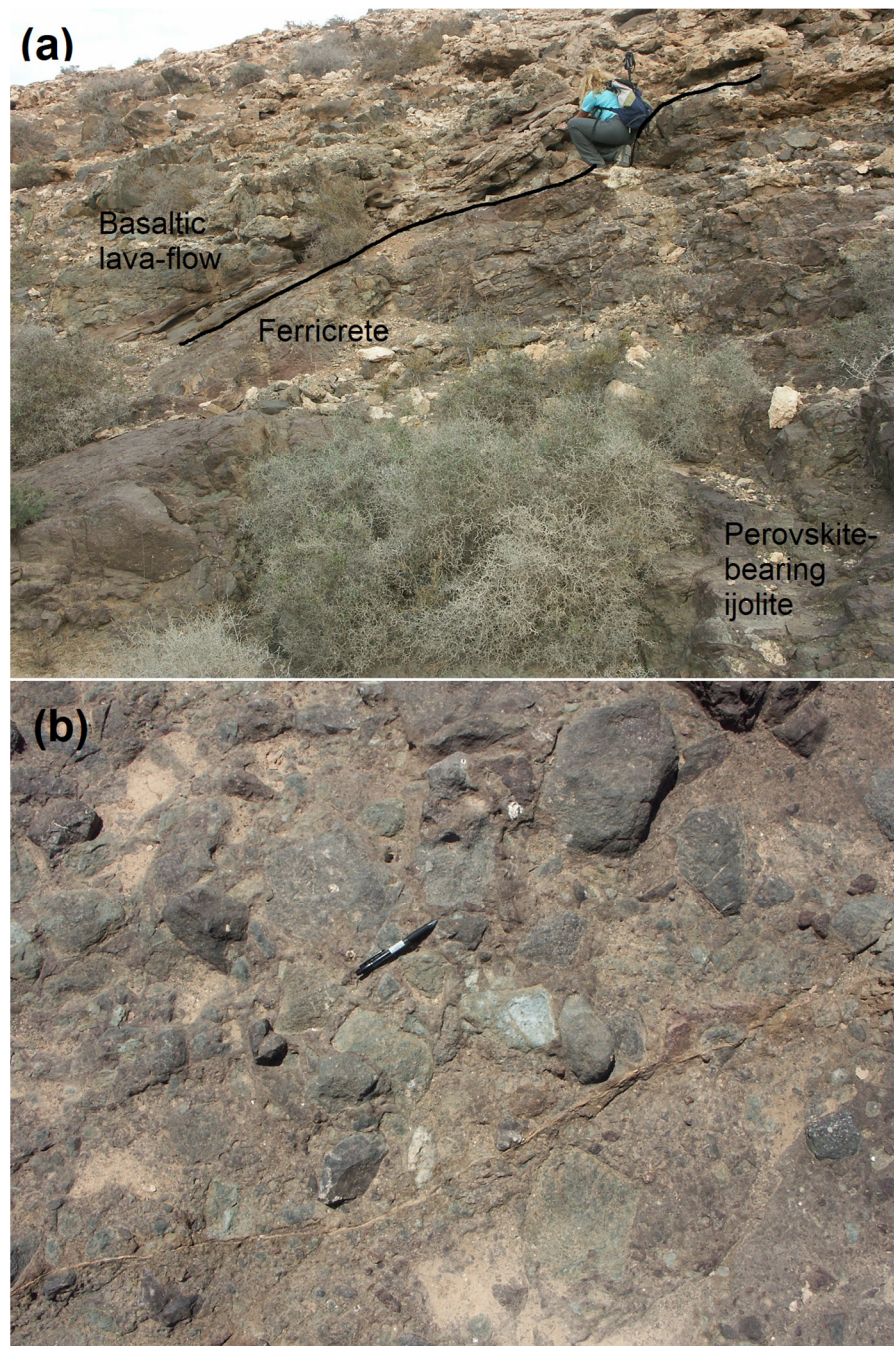


Figure 2. (a) Basaltic flows (Subaerial Volcanic Group–Initial Volcanic Ridge) lying unconformably over ferricrete produced by weathering of perovskite-bearing ijolites s. l. (Barranco del Agua Salada). (b) Detailed image of the ferricrete breccia with nephelinite, ijolite and syenite fragments cemented by a clayey-sandy matrix rich in iron oxides.

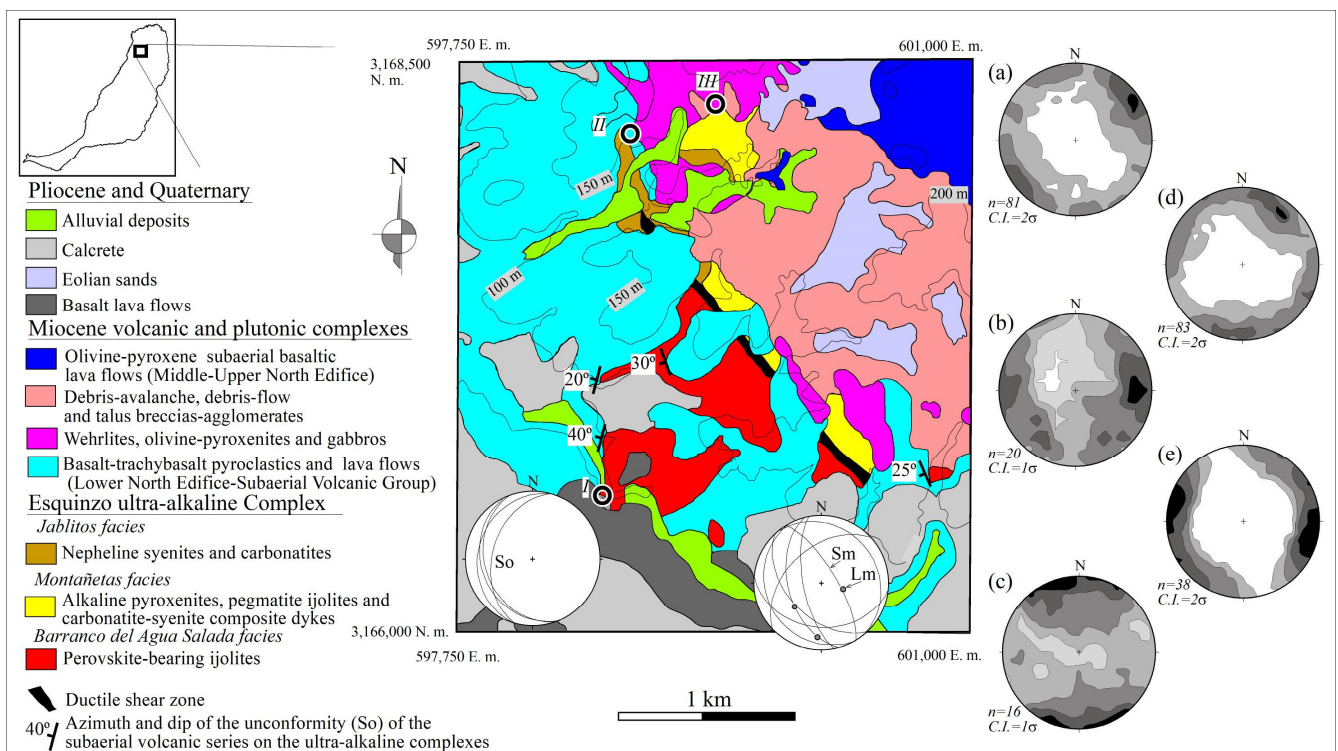


Figure 3. Detailed geological map of the central part of the area shown in Figure 1 (location in inset). Points I–III mark the location of the outcrops cited in the main text as representative of the intrusive relations between the Montaña Blanca–Montaña Milochó complex and the ultra-alkaline complex. Equal area, lower hemisphere projections of the unconformity (So) between the subaerial volcanic series (Subaerial Volcanic Group of the Initial Volcanic Ridge) and the ultra-alkaline complex, and of the mylonitic foliations (Sm) and lineations (Lm) in the ductile shear zone affecting the ultra-alkaline rocks. Density diagrams represent poles to (a) silicocarbonatite and (b) carbonatite dykes of the block to the NE of the ductile shear zone (Montañetas facies); (c) layering in perovskite-bearing ijolite (Barranco del Agua Salada Facies); (d) network of pinkish nepheline syenite dykes (Barranco del Agua Salada facies) and (e) nephelinite dykes and phonolitic nephelinites of the SW block ([54] method, $E = 3\sigma$, C.I.: contour interval, n: number of data).

The Esquinzo ultra-alkaline complex comprises alkaline pyroxenites, rocks of the melteigite-ijolite-urtite series, feldspathic ijolites, malignites and nepheline-syenites, silico-carbonatites, carbonatites (sövites and alvikites) and nephelinite/phonolitic dykes [18,33,55]. Rock types in the Esquinzo ultra-alkaline complex are very similar to nephelinite-clan carbonatites (represented by carbonatites associated with intrusive, melteigite-ijolite-urtite suite, nepheline syenite; and extrusive rocks: nephelinite, phonolite suite Ref. [5] or ijolite-nepheline syenite-carbonatite clan [56]: Napak in Uganda and Usaki (this one without carbonatites) and Kisingiri in Kenia [57] in the East African Rift). It is also similar to Fen in Norway, Alnö in Sweden, Spitzkop in South Africa, Lackner Lake in Canada and Magnet Cove in Arkansas. Nevertheless, in Esquinzo, phlogopite and perovskite pyroxenites are common. The Esquinzo plutonic complex could also be related to a nephelinite–ijolite association where carbonatites were found either with (h) melteigite-ijolite-urtite (no nephelinite extrusive rocks) or with (i) nephelinite in the classification defined by [58].

A major 100 m-wide anastomosing normal-dextral shear zone (see stereogram in Figure 3) divides the Esquinzo ultra-alkaline complex into two blocks showing important different lithological features (Figure 3). In the southwestern block, perovskite-bearing pyroxenites and perovskite-bearing melteigite-ijolite rocks cut by late nephelinite and phonolitic nephelinite dykes are predominant, while carbonatites occur in limited amounts. In contrast, in the northeastern block, there are no nephelinite or phonolitic nephelinite

dykes, but carbonatites, nepheline syenites and pegmatite ijolites are very abundant. In Figure 4, cross-cutting relationships between the different lithologies are shown in an E–W geological cross-section.

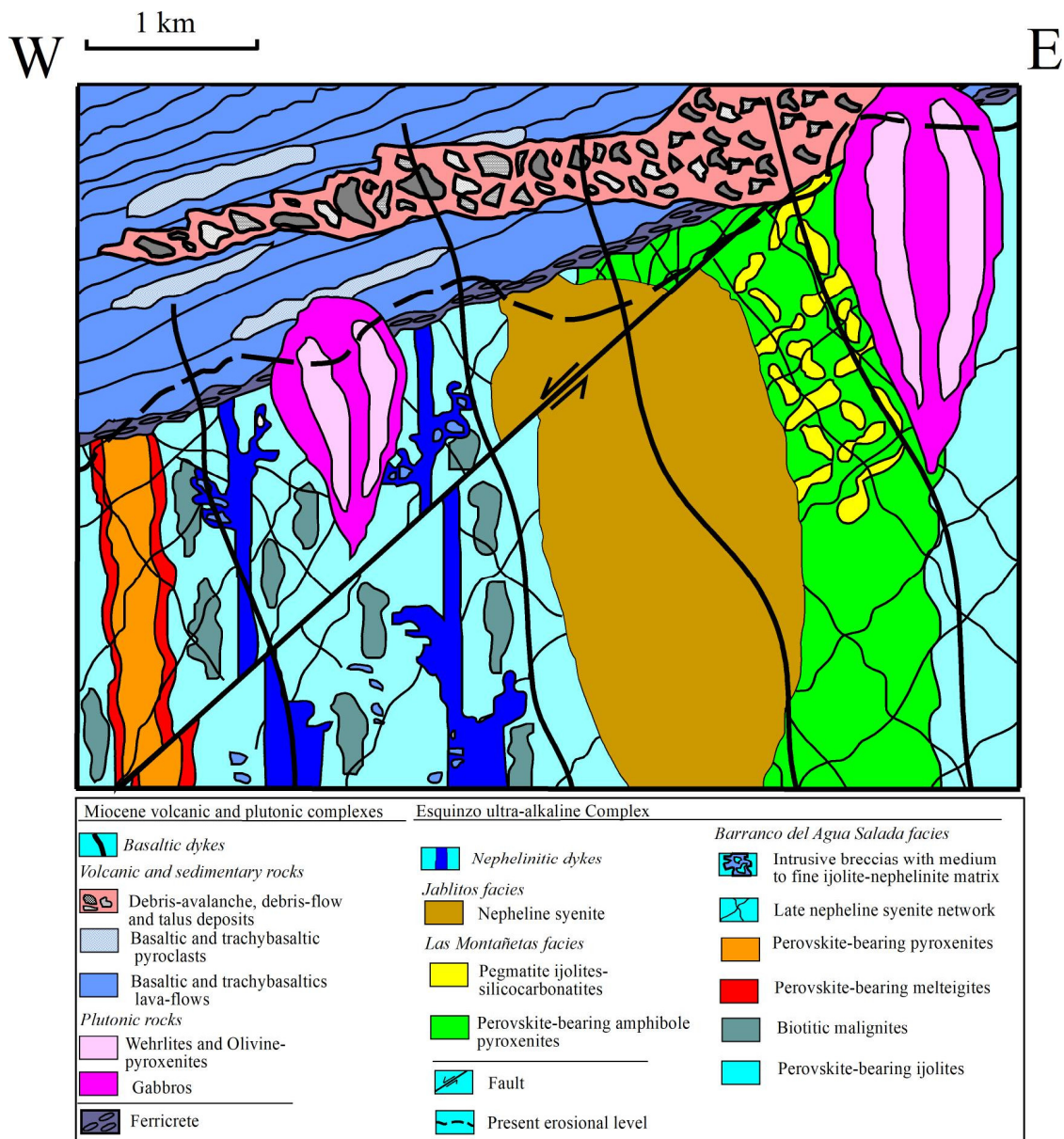


Figure 4. Cross-section, oriented W–E, of the central part of the area shown in Figure 1.

South of Playa de Esquinzo, another parallel reverse-sinistral shear zone occurs (Figure 1). Similar shear zones occur in the southern outcrops of this ultra-alkaline unit located in Caleta de la Cruz (Ajuy-Solapa) and Punta del Peñon Blanco [37,38].

1.2.1. Northeastern Block

The main outcrops are located in the north of the area shown in Figure 3. Two main rock associations appear here: Las Montañetas facies and Los Jablitos facies. Cross-cutting field relations indicate that the intrusive rocks of Los Jablitos area are younger than the lithologies of Las Montañetas. Some minor outcrops also occur around Montaña Los Frailes (Figure 1).

In Las Montañetas, the main rock types are perovskite-bearing amphibole pyroxenites and pegmatite ijolites grading into later nepheline syenite–silicocarbonatite–carbonatite

composite dykes (Figure 5a,b). Gradational contacts are pervasive throughout this outcrop. Perovskite-bearing amphibole pyroxenites are fine- to medium-grained rocks with blade texture, locally grading to melteigites and pegmatite ijolites. Pegmatite ijolites are the dominant lithology and form dykes in which long aegirine-augite prisms are usually arranged in a comb-texture perpendicular to the dyke margin (Figure 5c). These dykes seem to fill fractures in the pyroxenite bodies (Figure 5a). The pegmatite ijolites grade into feldspathic ijolites and subsequently into nepheline syenites and silicocarbonatites and carbonatites (Figure 5a,d).

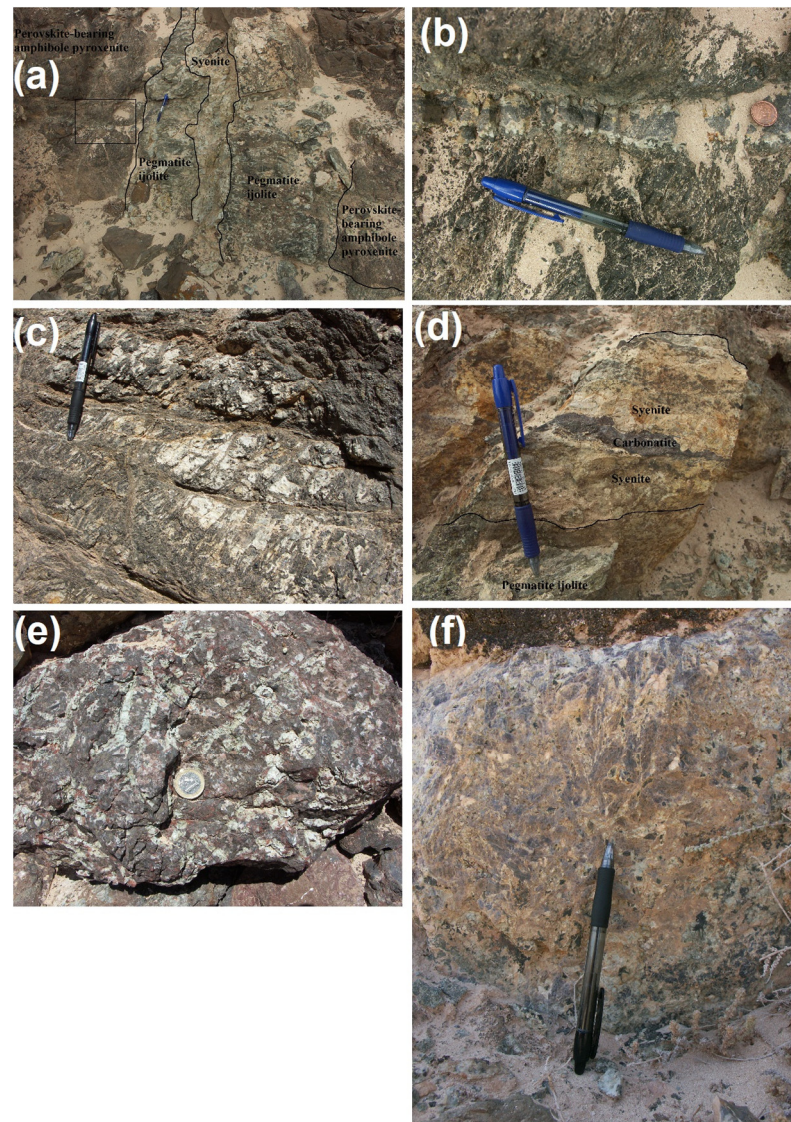


Figure 5. Photographs of the studied rocks. (a) Composite dykes (nepheline syenites in the inner part, pegmatite ijolites in the outer zone) cutting perovskite-bearing pyroxenites in Las Montañetas. The rectangle shows the location of Figure 5b. (b) Zoned dyke with inner carbonatite and syenite borders. (c) General aspect of a pegmatite ijolite dyke showing aegirine-augite crystals with comb-texture in Las Montañetas. (d) Composite dykes (inner carbonatite, outer syenite) inside pegmatite ijolites in Las Montañetas. (e) Textural aspect of Montaña Los Frailes carbonatites: large idiomorphic alkali feldspar crystals (white) with interstitial calcite (brown). (f) Carbonatite with tabular calcite crystals oriented parallel to a (0001) axis (grey) forming a three-dimensional network with all other minerals interstitial to the calcite crystals (white: nepheline and K-feldspar; black: pyroxene).

Silicocarbonatite and carbonatite dykes are usually subvertical and follow a NW–SE to N–S trend (Figure 3, density diagrams (a) and (b)). Secondary sets are NE–SW directed. Inside the shear zone these rocks are strongly foliated. A common feature of silicocarbonatite-carbonatite dykes is the occurrence of parallel bands with different mineralogy [18]. Silicocarbonatite-carbonatite dykes can form the inner part of meter-wide composite zoned dykes. The outer part of these dykes is formed by ijolite pegmatite, while the intermediate part consists of nepheline syenites. Alternatively, carbonatites occur in the inner part of narrow centimeter-wide nepheline syenite–carbonatite composite dykes (Figure 5d). A gradual transition between these rocks can be observed.

In some outcrops, spinifex textures can be observed in carbonatites, similar to those described by [59] as typical of non-recrystallized carbonatites. In these areas, tabular calcite crystals are oriented parallel to a (0001) axis and form a three-dimensional network with all other minerals situated between calcite crystals (Figure 5f). These textures have also been described by [60] in alvikites from the Dicker Willem (southwest Namibia) and in the Nooitgedacht carbonatite (Kaaopvaal Craton, South Africa) by [61]. Spinifex textures were interpreted as result of rapid growth, probably with some degree of supercooling [60], although [61] suggested they are a result of emplacement of a volatile-rich magma, forming a carbonatite pegmatite in the magma-chamber cupola.

In Los Jablitos, medium-grained nepheline syenites are dominant. They form a small sub-circular pluton, showing magmatic banding and large variations in both grain size and proportions of rock-forming minerals (nepheline, alkali feldspar and pyroxene). Mirolitic cavities were occasionally observed. Only occasionally are these rocks cut by fine-grained thin purple carbonatite veins composed entirely of calcite.

In Montaña de Los Frailes, medium-grained melteigites-ijolites-urtites are cut by some urtite dykes. These rocks are, in turn, intruded by a network of pyroxenitic and biotitic carbonatite veins (Figure 5e) and pinkish nepheline syenite dykes (late nepheline syenite network).

1.2.2. Southwestern Block

The main outcrops are located in the coastal area from Playa del Aguila to Playa de Tebeto (Figure 1) and at the center of the area mapped in Figure 3 (Barranco del Agua Salada Facies). Perovskite-bearing ijolite, with all transitions to melteigites and alkali pyroxenites, dominate the Barranco del Agua Salada Facies. They are greenish and show considerable mesoscopic variations in grain size and textural fabrics. Layering is locally defined by alternating bands marked by the accumulation of pyroxene and nepheline. The orientation of this layering is from E–W to ENE–WSW, and it appears mostly subvertical (Figure 3, density diagrams (c)).

These ijolites are systematically cross-cut by a network of pinkish nepheline syenite veins showing mainly NW–SE trends, with a secondary NE–SW azimuth (Figure 3, density diagrams (d)). These veins may be part of a slightly younger intrusion of nepheline syenite magma related to Los Jablitos intrusive body. In some areas, perovskite-bearing ijolites are also brecciated and cross-cut by later dykes of feldspathic ijolites (Montaña de la Morriña and Barranco del Agua Salada).

In the coastal area from Playa del Aguila to Playa de Tebeto, a complex set of lithologies can be found. The earliest and most abundant rocks are perovskite-bearing pyroxenites and melteigites-ijolites with very variable grain size (from medium- to very coarse-grained). Ijolitic rocks are usually younger than pyroxenites and melteigites. Occasionally, these three rock types form alternating bands with variable orientation. In melteigites and ijolites, the occurrence of areas rich in magnetite and biotite are common. In some areas, perovskite-bearing rocks (pyroxenites-melteigites-ijolites) are also brecciated and cross-cut by later dykes of feldspathic ijolites (Playa de Esquinzo). A network of thin microijolite dykes intrudes all these rocks.

South of Playa del Águila, ijolitic rocks grade locally into feldspathic ijolites and fine- or very coarse-grained biotitic malignites. Frequently the fine-grained types are hosted by

very coarse-grained feldspathic ijolites and malignites. All these lithologies are frequently cut by a network of pinkish nepheline syenite dykes showing mainly NW–SE trends.

This association is cut by intrusive breccias showing a fine- to medium-grained ijolite-nephelinite matrix with numerous fragments of pyroxenite, melteigite, medium-grained ijolite, feldspathic ijolite-malignite and pegmatite ijolite.

Late greyish green nephelinite and phonolitic nephelinite dykes cut all the lithologies found both on the coast and in Barranco de Agua Salada. They frequently contain ijolite fragments. These dykes are predominantly subvertical and N–S to NNE–SSW directed (Figure 3, density diagrams (e)).

2. Materials and Methods

The description of the methods used in the chemical analysis of the mineral phases and chemical analysis of selected rocks appears in the Text S1.

3. Results and Discussion

3.1. Petrography

The volumetric abundance of the main facies and also the petrographic key characteristics of the different rocks are summarized in Table 1. A more extensive petrographic description of the units can be found in the Text S2.

Table 1. Summary of the petrographic characteristics of the different rocks.

FACIES/Rocks	% Volume	Plutonic Event	Petrographic Characteristics
LAS MONTAÑETAS	15	1°	
Perovskite-bearing amphibole pyroxenites	70	1°	A prismatic pyroxene cumulate (80%) with brown interstitial Mg-hastingsite/pargasite in variable amounts (5%–10%). Minor brown phlogopite growing around pyroxenes (2%). Apatite forms interstitial aggregates (2%). Allotriomorphic perovskite (2%) includes crystals of apatite and titanomagnetite. Titanomagnetite has also an interstitial position (3%). Titanite crystals growing around perovskite (2%). Interstitial nepheline (2%). Pyroxene in the contact with interstitial nepheline has a slightgreenish pleochroism (diopside).
Pegmatite ijolite	20	1°	Feldspathic ijolites or even malignites grading to nepheline syenites. Coarse- to very coarse-grained size rocks frequently with comb texture defined by the orientation of large pyroxene (20%) crystals. Subidiomorphic brown micas grow over pyroxene. Nepheline (60%) and alkali feldspar (5%) are usually interstitial. Calcite (5%) is included into pyroxenes or fills interstices between other minerals. Apatite (1%) occurs as inclusions in pyroxene, perovskite (2%), biotite (2%), nepheline and alkali feldspar. Titanite (3%) grows interstitially between pyroxenes or around perovskite. Melanite (2%) occurs growing over titanite.

Table 1. Cont.

FACIES/Rocks	% Volume	Plutonic Event	Petrographic Characteristics
Nepheline syenites	5	1°	Form dykes or masses that grade from pegmatite ijolite to silicocarbonatites or carbonatites. They are medium- to coarse-grained rocks with a general texture defined by large idiomorphic alkali feldspar crystals (40%). Pyroxenes (10%) forming short prisms with calcite (1%) and apatite (1%) inclusions. Biotite (4%) and nepheline (40%) form subidiomorphic crystals. Calcite can form inclusions in pyroxene or fill interstices between alkali feldspars. In contact with alkali feldspar reaction rims composed of garnet, analcime and prehnite can be observed. Apatite, pyrochlore, zircon and titanite are common accessory phases (around the 1%).
Carbonatites and silicocarbonatites	5	1°	Coarse-grained sövites are dominant with variable content of silicate minerals. Occasionally silicates reach 50% of the rock (silicocarbonatites). Dykes with lower thickness and magnitude are usually fine- to medium-grained alvikites. In some outcrops spinifex textures can be observed in carbonatites. Calcite forms large platy subidiomorphic crystals commonly with consertal texture. Aegirine augite/aegirine form subidiomorphic crystals with many apatite and calcite inclusions. They occasionally occur intergrown with calcite. Biotite occurs as large primary idiomorphic crystals, frequently zoned. Subidiomorphic, very perthitic alkali feldspar crystals (sanidine) and nepheline also occur. Prismatic subidiomorphic or subrounded apatite inclusions are seen in sanidine, aegirine augite, biotite-phlogopite and calcite. Magnetite and Mn-rich ilmenite form discrete subidiomorphic crystals. Titanite is scarce and forms idiomorphic fractured crystals included into calcite and alkali feldspar. Pyrochlore forms zoned subidiomorphic crystals included in calcite (Supplementary Materials Figure S4b,d) and alkali feldspar. Monazite is included in apatite crystals or around it. Minor crystals of chalcopyrite, sphalerite and pyrite can be found.
LOS JABLITOS	5	2°	
Nepheline syenite	>99	2°	They can show both agpaitic or miaskitic textures. Are characterised by alkali feldspar (43%) and nepheline (43%), together with aegirine augite/aegirine (10%). Apatite (2%) and titanite (2%) are common accessory phases.

Table 1. Cont.

FACIES/Rocks	% Volume	Plutonic Event	Petrographic Characteristics
Carbonatite	>1	2°	Medium- to fine-grained alvikite dykes. They are dark pink or purple in color with calcite crystals (96%) full of hematite microexolutions. Apatite (4%) forms subrounded discrete grains or aggregates included or placed around calcite margins.
MONTAÑA DE LOS FRAILES	5	1° and 2°	
Melteigites-ijolites-urtites	90	1°	Biotite melteigites are dominant and grade locally to ijolites-urtites. The overall rock microstructure of these rocks is that of a prismatic pyroxene cumulate. Pyroxene crystals are subidiomorphic and frequently zoned showing a pink core (titanian diopside) and pale green or uncolored rims (diopside). Minor brown biotite also occurs in some samples growing around pyroxenes. Apatite and titanomagnetite are ubiquitous. Some samples contain titanite, nepheline, andradite garnet and calcite.
Carbonatites	5	1°	Calcite crystals (80%) include prismatic alkali feldspar (10%), idiomorphic titanite (3%, ore-rich rims), red pleochroic idiomorphic biotite plates (3%) and prismatic apatite crystals (4%), both isolated and as aggregates.
Nepheline syenite network	50	2°	Late nepheline syenites form a network of pinkish dykes and veins. Hetero granular rocks with coarse to very coarse grain size and frequently showing comb textures due to the orientation of alkali-feldspar (43%) and pyroxene (10%) aggregates. Nepheline (43%) and fractured zircon grains (4%) commonly occur.
BARRANCO DEL AGUA SALADA. 75%. 1°, 2° and 3° Plutonic Events	75	1°, 2° and 3°	
Alkali pyroxenites	35	1°	Alkali pyroxenites grading to melteigites are predominantly medium- to coarse-grained rocks containing usually phlogopite and perovskite (Playa de Esquinzo) or amphibole (Playa de Tebeto). They are commonly accumulated to mesocumulates with clinopyroxene (75%, titanian diopside and diopside), kaersutitic amphibole (8%), subidiomorphic perovskite (3%) and idiomorphic apatite (3%) as cumulus phases, while phlogopite (2%), titanomagnetite (2%), titanite (1%), nepheline (3%) and calcite (3%) are intercumulus minerals.

Table 1. Cont.

FACIES/Rocks	% Volume	Plutonic Event	Petrographic Characteristics
Perovskite-bearing ijolites s.l	50	1°	Perovskite-bearing ijolites s.l. are meso to orthocumulates, with the nepheline/clinopyroxene ratio increasing from melteigite (3:1) to ijolite (1:3). They also contain brown phlogopite (3%) and kaersutite (3%), abundant apatite (2%), magnetite (2%), perovskite (2%) and allotriomorphic titanite (2%) is seen in place of perovskite. In urtitic ijolites, the occurrence of interstitial melanite crystals (4%) is common.
Biotitic malignites (feldspathic ijolite-biotitic malignites-nepheline syenites)	5	1°	In fine-grained types, the rock texture is characterized by the presence of poikilitic crystals, both idiomorphic (titanite and zoned biotite) and allotriomorphic (nepheline, alkali feldspar and calcite), containing small idiomorphic zoned pyroxene crystals (titanian diopside, diopside and aegirine augite), apatite and titanomagnetite. Inside the biotite crystals colorless cores and outer rims with strong red-brown pleochroism are observed. In coarse- to very coarse-grained varieties, textures are equigranular with large idiomorphic zoned pyroxene (titanian diopside, diopside and aegirine augite), apatite, titanite, perovskite and biotite (Supplementary Material Figure S5b). Nepheline, alkali feldspar (Supplementary Material Figure S5c) and calcite occur interstitially. Biotite forms large crystals growing over or as aggregates around pyroxenes. Nepheline is subidiomorphic and occurs interstitially or as inclusions in alkali feldspar
Feldspathic ijolite veins	<1	1°	Contain aegirine augite (20%) and crystals of zoned nepheline (50%), which is invariably highly altered and pinkish or almost red in color. Pyroxene and nepheline are enclosed by clear “pools” of interstitial or poikilitic alkali feldspar (20%). Orange-brown phlogopite (11%) is also common. Accessory minerals include titanite (3%), apatite (3%) and magnetite (3%).
Late nepheline syenite network	<3	2°	Network of pinkish dykes and veins that cut all the lithologies They are heterogranular rocks with coarse to very coarse grain size frequently with comb texture due to the orientation of alkali-feldspar (60%) and pyroxene (20%) aggregates. Also include heavily altered nepheline (11%), fractured zircon grains (3%), idiomorphic pyrochlore crystals (3%) and biotite (3%).

Table 1. Cont.

FACIES/Rocks	% Volume	Plutonic Event	Petrographic Characteristics
Intrusive breccias with medium- to fine-grained ijolite-nephelinite matrix	<1	3°	Heterogeneous porphyritic rocks containing abundant fragments of xenocrysts and different rock types. The most common phenocrysts are subidiomorphic (diopside and titanian diopside) pyroxenes (30%) and heavily altered nepheline (60%). Biotite phenocrysts (10%) also occur occasionally. The groundmass contains small nepheline and calcite crystals interstitially or as ocelli.
Nephelinite and phonolitic nephelinite dykes	<5	3°	Nephelinite and phonolitic nephelinite dykes constitute the youngest intrusions. They are strongly porphyritic with pyroxene (50%), nepheline (40%), red-brown garnet (3%), alkali feldspar (3%) and titanite phenocrysts (2%) and minor amounts of oxide minerals (2%). The groundmass consists mainly of fine-grained pyroxene, alkali feldspar, nepheline and titaniferous magnetite. Accessory minerals include apatite, titanite and perovskite.

In summary, field relations among the different lithologies and petrographic study of all the rock types indicate the presence of at least three independent and consecutive magmatic pulses (Text S2) [62]:

- (1) The early magmatic event (Plutonic Event 1) formed the rocks of Las Montañetas Facies (perovskite-bearing amphibole pyroxenites, pegmatite ijolite, nepheline syenites, silicocarbonatites and carbonatites), Montaña Los Frailes Facies (melteigites-ijolites-urtites and carbonatites) and most of the rocks forming Barranco del Agua Salada Facies (perovskite-bearing pyroxenites, perovskite-bearing ijolites s.l., biotitic malignites and the feldspathic ijolite veins of Playa de Esquinzo and Montaña de la Morriña).
- (2) A second magmatic pulse (Plutonic Event 2) formed Jablitos Facies (nepheline syenites), late feldspathic ijolite veins (Barranco del Agua Salada) and the nepheline syenite network in Barranco del Agua Salada, Montaña Los Frailes and Playa del Águila.
- (3) The third magma batch (Plutonic Event 3) formed the nephelinite and phonolitic nephelinites dykes and the intrusive breccias with medium- to fine-grained ijolite-nephelinite matrix found in Barranco del Agua Salada Facies.

3.2. Mineral Chemistry

Here, we describe the chemical composition of the main mineral phases found in the Esquinzo ultra-alkaline complex, together with P and T estimates of the formation of the minerals and magma evolution.

3.2.1. Pyroxene

Selected and representative compositions of pyroxenes, calculated according to [63], are shown in Table S1. They are mainly calcic (diopside and occasionally hedenbergite) or calcic-sodic pyroxenes (aegirine-augite) with low Ni and Cr contents. All have very low Al^{VI}, resulting in insignificant amounts of jadeite and Ca-Tschermaks (CATS), which indicates a low pressure crystallization. Most of the compositional variations can be described in terms of Ti-Tschermaks (CTTS), Fe-Tschermaks (CFTS) and aegirine substitutions.

Distinct alkaline clinopyroxene trends are generally believed to show consanguinity of various rocks of alkaline complexes [64–67]. Next, we will characterize pyroxenes from the three different intrusive stages (Figure 6).

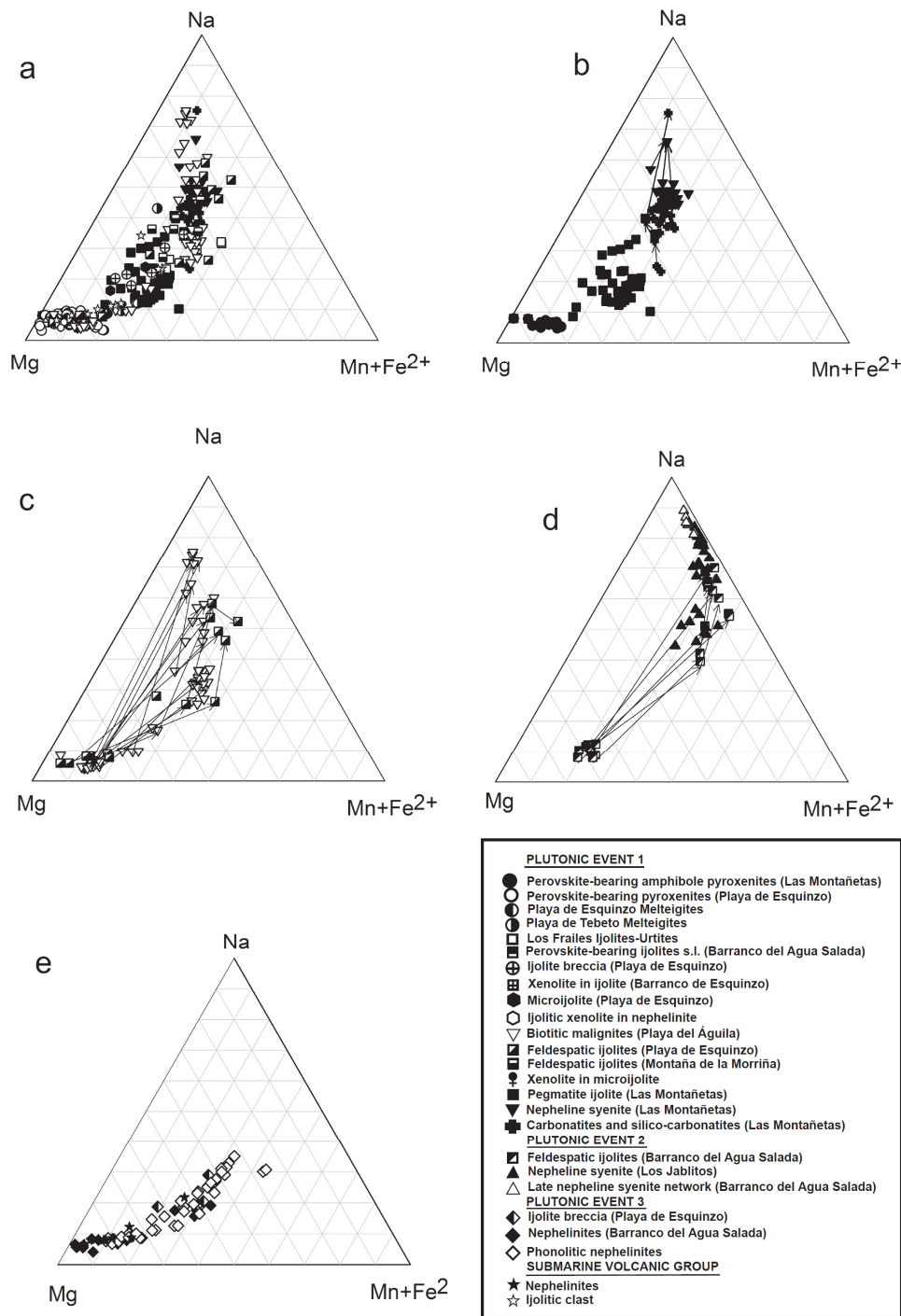


Figure 6. Na–Mg–Mn+Fe²⁺ compositional variation diagrams of pyroxenes from the ultra-alkaline Esquinzo complex (data are plotted in cations per formula unit). (a): 1st Plutonic Event, all places and rocks. (b): 1st Plutonic Event at Las Montañetas. (c): 1st Plutonic Event, biotite malignites and feldspathic ijolites. (d): 2nd Plutonic Event. (e): 3rd Plutonic Event. The arrows show zoned crystals from core to rim.

In Plutonic Event 1, pyroxenes from the less evolved, more mafic, rocks (Figure 6a), i.e., perovskite-bearing amphibole pyroxenites from Las Montañetas, perovskite-bearing

melteigites-ijolites from Barranco del Agua Salada, Playa de Tebeto melteigites and perovskite-bearing pyroxenites from Playa de Esquinzo, are all diopsides with relatively high TiO₂ contents (up to 3.44 wt%). Clinopyroxene shows a wide compositional range (Figure 6) as differentiation increases and the modal composition of the rocks varies i.e., as nepheline and alkali feldspar increase, while the mafic phases decrease (amphibole, pyroxene, perovskite, etc.). For example, pegmatitic ijolites for Las Montañetas show wide compositional variations from ijolites to feldspathic ijolites-malignites. Ijolitic rocks contain diopside with up to 1.45 wt% TiO₂, while pyroxene in feldspathic ijolite-malignite rocks is aegirine-augite. Compositional zonation with an increase in aegirine contents occurs from crystal core to rim (Figure 6b). Pyroxenes from nepheline syenite-carbonatite composite dykes show a similar composition in both the carbonatite and syenite parts. They are also aegirine augite, generally with higher acmite contents (Figure 6b). They show compositional zoning with increasing aegirine contents from core to rim (Figure 6b).

Ijolites and feldspathic ijolites s.l. from other sectors of the Esquinzo complex, belonging to the first and second Plutonic Events, show similar trends, starting with diopside-rich pyroxene compositions evolving toward more hedenbergite (Hed) and acmite-rich compositions with progressive differentiation (Figure 6).

Pyroxenes in Playa del Águila malignites and feldspathic ijolites from Playa de Esquinzo (Figure 6c) also show compositional and color zoning: from pink cores to dark green rims through intermediate light green zones. This coincides with the zoning observed in pyroxenes from the first magmatic stage, starting with diopside-rich pyroxene compositions evolving toward more hedenbergite and acmite-rich compositions with progressive differentiation. This zoning can be characterized by Mg-loss, substituted either by Fe²⁺ (almost exclusively) or by Na + Fe³⁺. The first trend is similar with that of observed in pyroxenes from nepheline syenite-carbonatite composite dykes from Las Montañetas (Figure 6b), the second one is dominant in zoned pyroxenes from the second Plutonic Event (Figure 6d). The compositional gap between pink cores and green rims seems to indicate a hiatus in pyroxene growth.

Clinopyroxenes from ijolite fragments found in the lower part of the S.V.G [25] overlap the compositional range of pyroxenes found in pyroxenites-ijolites from the first magmatic stage (Figure 6a).

Pyroxenes from the second magmatic stage feldspathic ijolites from Barranco del Agua Salada, nepheline syenite from Los Jablitos and late pinkish nepheline syenite network show a different evolution to that observed for pyroxenes from the first stage with greater Fe²⁺ enrichment (Hed) while evolving toward acmite composition (Figure 6d). Pyroxenes in Los Jablitos nepheline syenites and related late pinkish nepheline syenite veins (Plutonic Event 2) are aegirine augites and aegirines with increasing aegirine contents from core to rim. They show the highest acmite contents in the whole Esquinzo Complex (Figure 6b). Pyroxenes from feldspathic ijolites from Barranco del Agua Salada show zoning from pink cores (diopside) to dark green rims (aegirine augite—aegirine) that follows the general compositional evolution of pyroxenes of this second magmatic stage (Figure 6d). The compositional gap between pink cores and green rims indicates a hiatus in pyroxene growth. These variations suggest differences in oxidation state of the parental magma, so that magma of Plutonic Event 2 probably crystallized under less oxidized conditions compared with magma from Plutonic Event 1 [67,68].

Pyroxenes in ijolitic breccia (Playa de Esquinzo), phonolitic nephelinite and nephelinite dykes (Plutonic Event 3) have nearly pure diopside compositions with TiO₂ between 2.28–4.28 wt%. Clinopyroxene phenocrysts in nephelinite lavas from the S.V.G. [26] have a similar composition to pyroxene phenocrysts in rocks of this third Plutonic Event (Figure 6). Pyroxene phenocrysts from phonolitic nephelinites are generally aegirine augite (Figure 6e). Crystals frequently show zoning, either simple or complex. In some crystals, cores are beige-brown or pale green diopside with aegirine augite rims, whereas others show an apple-green aegirine augite core, an intermediate pale green diopside zone and, again, an outer apple-green aegirine augite rim. Other phenocrysts show an inverse situation

with cores and outer beige-brown to light green diopsidic rims and a middle apple-green aegirine augite zone.

In summary, clinopyroxene from this youngest magma batch (Plutonic Event 3) also formed an uninterrupted trend from diopside to acmite in the Mg-Na-(Fe²⁺+Mn) ternary diagram (Figure 6e).

3.2.2. Micas

Mica occurs in many rocks of the first magmatic stage: perovskite-bearing amphibole pyroxenites, pegmatite ijolites, nepheline syenite–carbonatite composite dykes, feldspathic ijolites from Las Montañetas Facies, in ijolite-urtites from Montaña Los Frailes and in rocks from Barranco del Agua Salada Facies (coastal outcrops): perovskite-bearing pyroxenite-melteigites from Playa de Esquinzo and malignites from Playa del Aguila. Mica is absent in Los Jablitos nepheline syenites of the second magmatic stage but occurs as an accessory mineral in the late pinkish nepheline syenite veins.

Representative analyses are presented in Table S2. In general, micas are Ti-bearing phlogopite-biotites with normal pleochroism. Micas in Playa del Aguila malignites show strong zoning, from light brown/colorless cores to dark brown rims. In contrast, those in carbonatite-nepheline syenite composite dykes from Las Montañetas have reverse zonation with dark brown cores and light brown rims (Figure 7b–d). In malignite micas, zoning is marked by a decrease in Ti and Al contents as the Fe²⁺/Fe²⁺+Mg ratio increases (Figure 7b–d). This trend, from phlogopite to biotite, overlaps the general compositional evolution of micas in rocks in Plutonic Event 1 from pyroxenites-melteigites to ijolite-feldspathic ijolites (Figure 7a–c). On the other hand, these patterns are accompanied by an increase in the Mn content of micas (Figure 7e,f). These trends can be explained by a decrease in Ti and Al contents and by a slight increase of Mn available in the magma during differentiation. Thus, in perovskite-bearing amphibole pyroxenite from Las Montañetas, mica is a phlogopite with up to 3.24 wt% TiO₂. Perovskite-bearing pyroxenites and melteigites from Playa de Esquinzo also have phlogopites (3.39–5.35 wt% TiO₂) containing appreciable amounts of BaO (up to 1.28 wt%) and high Na₂O contents (up to 0.91 wt%).

Feldspathic ijolites from Playa de Esquinzo and Montaña de la Morriña contain titanian biotites (2.4–3.24 wt% TiO₂) with the highest MnO contents (0.94–1.52 wt%) of the Esquinzo complex. They contain microxenoliths of a biotite micromelteigite in which biotite has a similar composition to that of the host rock.

Micas from nepheline syenite–carbonatite composite dykes have variable TiO₂ contents (1.56–3.98 wt%), up to 1.44 wt% BaO and 0.38–0.99 wt% MnO. Al₂O₃ contents are low (10.37–11.75 wt%), as is typical for phlogopite from carbonatites [69]. In these rocks, mica shows a more complex evolution trend. Zoning indicates a moderate Al increase and a decrease of Ti and Mn contents as Fe²⁺/Fe²⁺+Mg ratio decrease (Figure 7b,d,f).

Varying Fe²⁺/Fe²⁺+Mg values of micas depend on the composition of the host silico-carbonatite magma and on the presence or absence of magnetite crystallizing from it [70]. In this way, during mica crystallization in the nepheline syenite–carbonatite composite dykes, the Fe²⁺/Fe²⁺+Mg ratio decreases continuously. The decrease of iron in the mica could be correlated with increasing oxygen fugacity in the silico-carbonatite magma, with a consequent increase in the Fe³⁺/Fe²⁺ ratio, building up to precipitation of magnetite at the rims of many mica grains.

In the second magmatic stage, micas are scarce. We have only observed some biotite crystals in the late pinkish nepheline-syenite network. They have relatively high TiO₂ contents (3.12–3.63 wt%).

Micas in ijolite xenoliths or as xenocrysts included in Volcanic Submarine Group nephelinite lavas [25] are similar in composition to phlogopites from the ultramafic rocks of the Esquinzo ultra-alkaline complex.

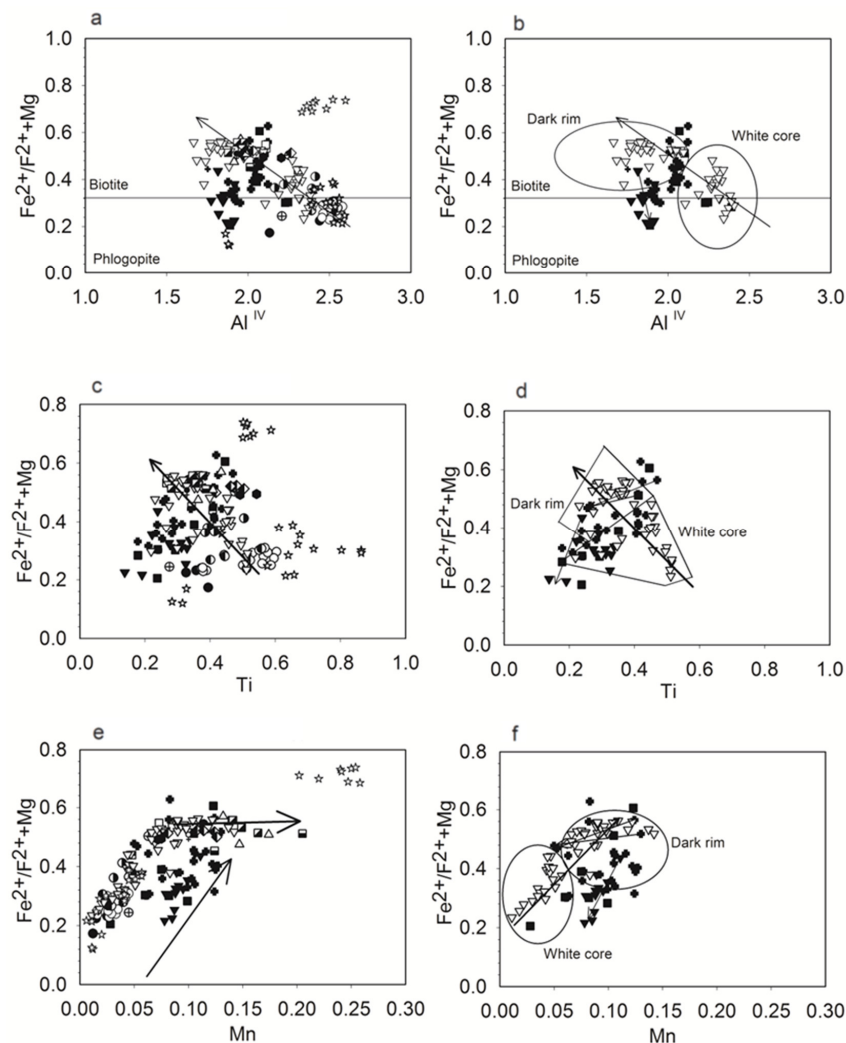
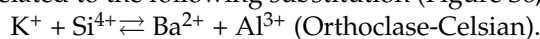


Figure 7. Compositional variation diagrams of micas from the ultra-alkaline Esquinzo complex (data are plotted in cations per formula unit). The arrows mark the differentiation process. (a): $\text{Fe}^{2+}/\text{Fe}^{2+}+\text{Mg}$ vs. Al_{tot} for all rocks. (b): $\text{Fe}^{2+}/\text{Fe}^{2+}+\text{Mg}$ vs. Al_{tot} for biotitic malignites, pegmatite ijolites, nepheline syenites, carbonatites and silico-carbonatites. (c): $\text{Fe}^{2+}/\text{Fe}^{2+}+\text{Mg}$ vs. Ti for all rocks. (d): $\text{Fe}^{2+}/\text{Fe}^{2+}+\text{Mg}$ vs. Ti for biotitic malignites, pegmatite ijolites, nepheline syenites, carbonatites and silico-carbonatites. (e): $\text{Fe}^{2+}/\text{Fe}^{2+}+\text{Mg}$ vs. Mn for all rocks. (f): $\text{Fe}^{2+}/\text{Fe}^{2+}+\text{Mg}$ vs. Mn for biotitic malignites, pegmatite ijolites, nepheline syenites, carbonatites and silico-carbonatites. Symbols as in Figure 6.

3.2.3. Feldspar

Feldspar occurs in many rocks of the Esquinzo complex (Figure S6). It is a rock-forming mineral in nepheline syenites, phonolite nephelinites, feldspathic ijolites-malignites, silico-carbonatites and carbonatites and occurs in variable amounts in pegmatite ijolite. Almost all are orthoclase-sanidine (Table S3, Figure S6, Ab-Or-An diagram). Only some heavily altered feldspars show higher Ab contents (Figure S6, Ab-Or-An diagram). The highest BaO contents were found in the feldspars from Los Jablitos nepheline syenites (2.14 and 6.03 wt%) and from nepheline syenite-carbonatites composite dykes (silicocarbonatites) from Las Montañetas (1.08 and 2.79 wt%). Entry of Ba into the feldspar structure seems to be related to the following substitution (Figure S6, K-Ba diagram):



3.2.4. Nepheline

Most nepheline crystals in the Esquinzo ultra-alkaline complex have been transformed to zeolites by low-temperature hydrothermal alteration. Only in the nepheline syenites from Los Jablitos and the phonolitic nephelinites was it possible to analyze unaltered nepheline crystals. In the Los Jablitos nepheline syenites, nepheline compositions vary between $Ne_{69.72} Ks_{18.23} Qtz_{12.05}$ and $Ne_{72.85} Ks_{19.31} Qtz_{7.84}$, while in phonolitic nephelinites, nepheline compositions change from $Ne_{73.15} Ks_{20.57} Qtz_{6.28}$ to $Ne_{70.20} Ks_{22.09} Qtz_{7.71}$ (Table S4, Figure S7, Ne-Ks-Qtz diagram). Interpolation in Hamilton's diagram (Figure S7, Ne-Ks-Qtz diagram, [71]) gives a slightly higher crystallization temperature for nephelines found in nepheline syenites from Los Jablitos (between 775 °C and more than 1058 °C) than nephelines crystals from phonolitic nephelinite (between 700 °C and 1058 °C).

3.2.5. Garnet

Igneous garnet occurs in some pegmatite ijolites from Las Montañetas, in Montaña de Los Frailes ijolite-urtites, in malignites from Playa del Aguila and in phonolitic nephelinite dykes. In pegmatite ijolite it forms large dark red-brown or black anhedral crystals. In phonolitic nephelinites garnet occurs as euhedral, brown phenocrysts but also in the groundmass. Their compositional range (Table S5 and Figure 8) covers that of garnets from other igneous rocks from Fuerteventura Basal Complex in ijolites [33] and in nephelinite submarine lavas [25].

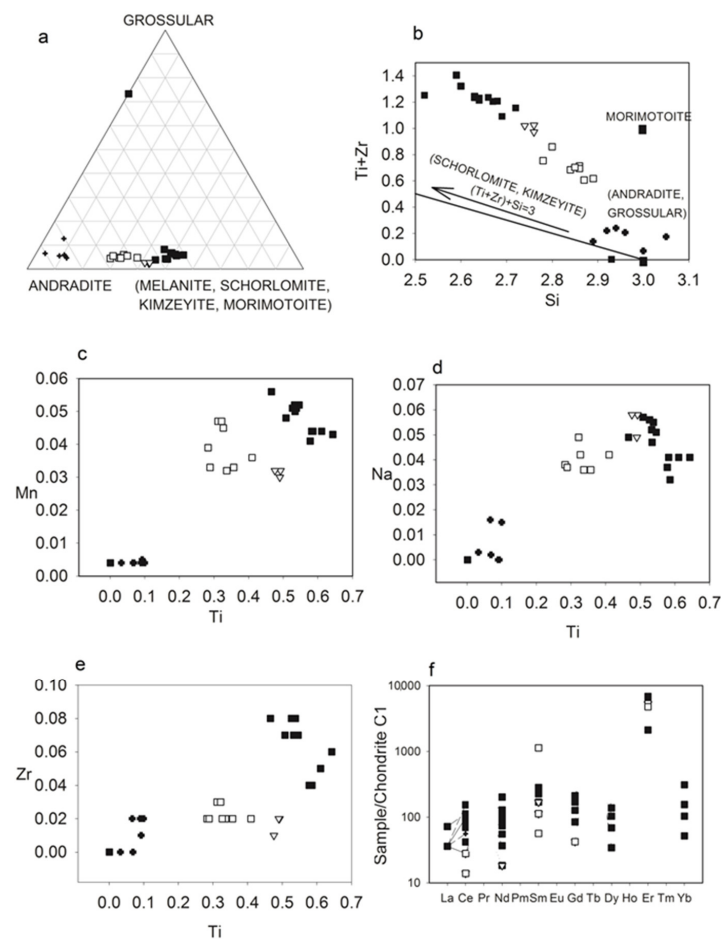
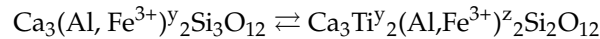


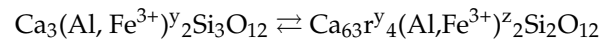
Figure 8. Compositional variation diagrams of garnets from the ultra-alkaline Esquinzo complex (data are plotted in garnets components (a), in cations per formula unit (b–e) and CI-chondrite-normalized REE patterns (f), normalization values from [72]). Symbols as in Figure 6.

The igneous garnets ($X_6 Y_4 Z_6 O_{24}$) are mainly grandites (grossular-andradite; X is filled by Ca, and Y is mainly occupied by Al^{VI} and Fe^{3+VI}) with remarkable Ti and Zr contents (Table S5 and Figure 8; $Al^{VI}-Fe^{VI3+}-Ti+Zr$, (Grossular-Andradite-(Melanite, Schorlomite, Kimzeyite and Morimotoite)), ternary diagram). Ti and Zr enter the structure through the following substitution mechanisms:

(a) Grandite \rightleftharpoons Schorlomite:

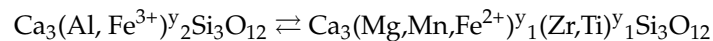


(b) Grandite \rightleftharpoons Kimzeyite:



and

(c) Grandite \rightleftharpoons Morimotoite:



In these reactions, Ca represents ions at the 'X' site (Ca, Fe^{2+x}, Mg^x, Mn^x) and is invariant.

In reactions (a) and (b), Al and Fe^{3+} pass from 'Y' to 'Z'; however, their quantities do not change. If Ti and Zr entered garnet only by the schorlomic and kimzeyitic substitutions, respectively, then the following relation would be valid:

$$(Ti + Zr) + Si = 3$$

However, the quantity of Ti + Zr exceeds this ratio in most cases (see in Figure 8b, the Ti + Zr vs. Si diagram), indicating the presence of morimotoitic substitution. The darkest garnet crystals found in pegmatite ijolites from Las Montañetas have the highest ZrO_2 and high TiO_2 contents (Table S5 and Figure 8, $Al^{VI}-Fe^{VI3+}-Ti + Zr$, (Grossular-Andradite-(Melanite, Schorlomite, Kimzeyite and Morimotoite)), ternary diagram), reaching about 55 wt% mol-wt% (Morimotoite, Schorlomite, Melanite and Kimzeyite).

Garnets from biotitic malignites from Playa del Águila show a 45 wt% mol-wt% morimotoite, schorlomite, melanite and kimzeyite components, while the garnets of the ijolites-urtites of Los Frailes zone have between 25 wt% and 40 wt% of morimotoite-schorlomite-melanite and kimzeyite components.

High Na_2O contents (up to 0.59 wt%) are characteristic of these garnets and a common feature of garnets in many peralkaline syenites and ijolites [73]. The authors of [74] pointed out that the presence of Na in the garnets from peralkaline igneous rocks is possibly due to appropriate bulk chemistry control favoring the coupled $NaTi-CaFe^{3+}$ substitution [75] (Figure 8, Ti-Na diagram).

The content in MnO is also significant, ranging from to 0.07 to 0.97 wt%. There is a good correlation between Mn and Ti contents in the analyzed crystals (Figure 8, Ti-Mn diagram).

Most grains are zoned with dark cores overgrown by lighter rims. The dark cores are relatively rich in TiO_2 , MgO and Al_2O_3 , but lower in total FeO and SiO_2 . These dark core-light rim chemical characteristics are found in zoned Ti-andradites from other alkaline rocks [25,74,76].

Chondrite-normalized rare earth element (REE) compositions of the garnets analyzed are shown in the Figure 8. They are enriched in HREE compared with LREE and show upward chondrite-normalized patterns.

In silicocarbonatites and pegmatite ijolites from Las Montañetas, some colorless metamorphic garnets occur. These are characterized by a high grandite component with low Ti, Zr, Mn and Na (Figure 8).

3.2.6. Carbonates

Carbonates are rock-forming minerals in carbonatites but also occur as accessories in various lithologies: nepheline syenite–carbonatite composite dyke (silicocarbonatites) from Las Montañetas, Los Frailes ijolites-urtites, perovskite-bearing ijolites from Barranco del Agua Salada, biotitic malignites from Playa del Águila, feldspathic ijolites from Montaña de la Morriña (Plutonic event 1) and the late nepheline syenite network (Plutonic event 2). Almost all crystals are calcites s.s. with high Sr contents (Table S8 and Figure 9). Only occasionally Ca-Mg-bearing carbonates were found in a nepheline syenite from Las Montañetas (Mg-Calcite) and also in a vein from the late nepheline syenite network (dolomite). Calcites from all the rock types have similar Mn and Sr contents (Table S8).

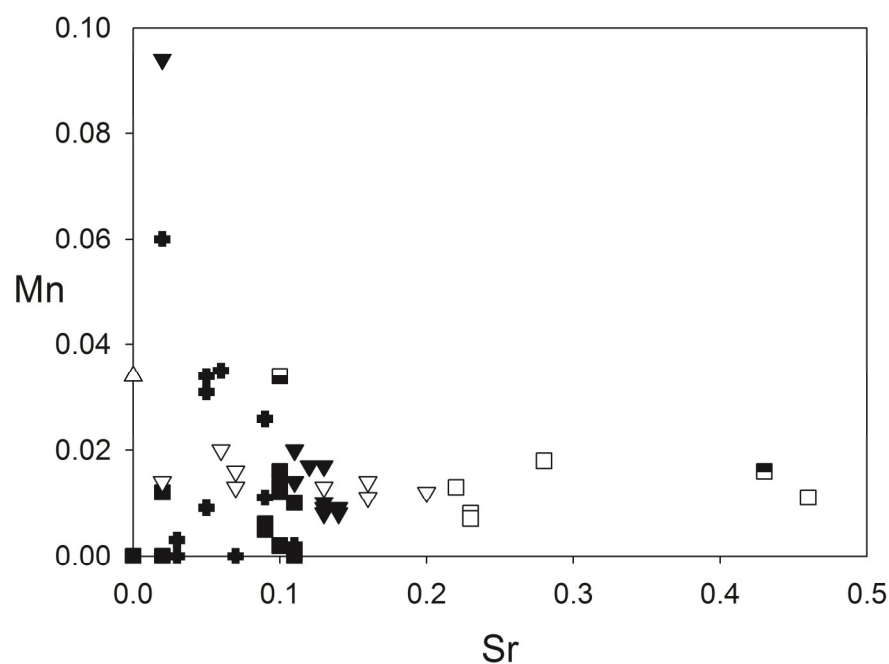


Figure 9. Compositional variation diagram of carbonates from the ultra-alkaline Esquinzo complex (data are plotted in cations per formula unit). Symbols as in Figure 6.

3.2.7. Magnetite and Ilmenite

Ilmenite (FeTiO_3) in the ultra-alkaline Esquinzo complex show moderate pyrophanite (MnTiO_3) and geikelite (MgTiO_3) contents (Table S10a; Figure 10). Magnetite (Fe_3O_4) contains small amount of ulvöspinel (TiFe_2O_4) and spinel (MgAl_2O_4). Its high jacobsite ($\text{Mn}^{2+}(\text{Fe}^{3+})_2\text{O}_4$) and magnesioferrite ($\text{Mg}(\text{Fe}^{3+})_2\text{O}_4$) contents are remarkable (Table S10b, Figure 10).

The description of the chemical characteristics of amphiboles, titanites, apatites, perovskites and pyrochlores found in the Esquinzo ultra-alkaline complex appears in the Text S3 (Figures S8–S12, Tables S6,S7,S9,S11 and S12) [77–87].

3.3. Geochemistry

Representative whole rock analyses of the most common lithologies found in Esquinzo ultra-alkaline complex are given in the Table S13. Samples have been selected from the main outcrops: Playa de Esquinzo (perovskite-bearing pyroxenite, melteigites and nephelinites/nepheline phonolite dykes), Playa del Aguila (ijolites, feldspathic ijolites and malignites), Las Montañetas (perovskite-bearing amphibole pyroxenite, pegmatite ijolite, nepheline syenite–carbonatite composite dykes and carbonatites), Los Jablitos (nepheline syenite) and Barranco del Agua Salada (medium-grained perovskite-bearing ijolite, carbonatite dykes and nephelinite/nepheline phonolite dykes). Data presented by [3,33] are also included in this study for comparison.

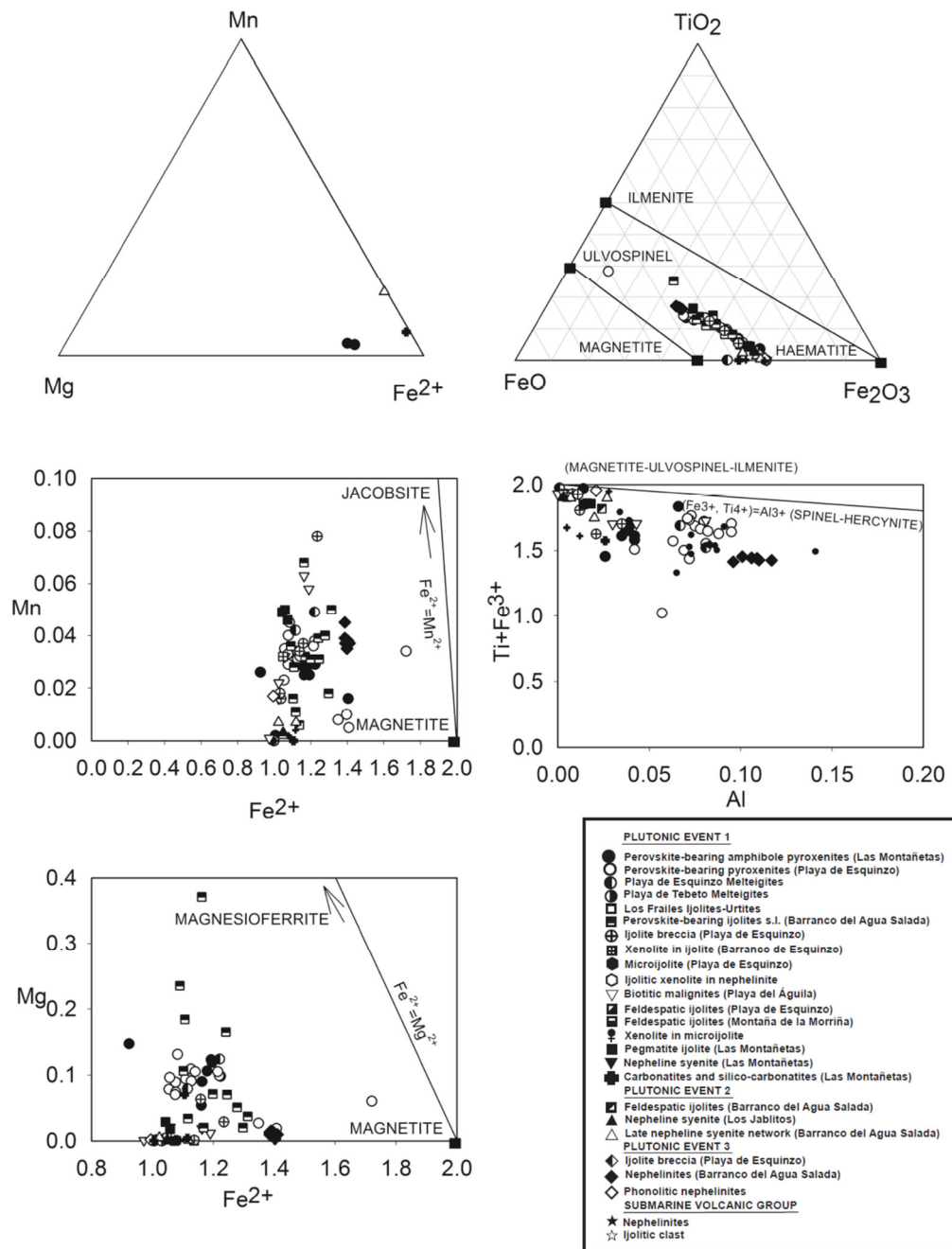


Figure 10. Compositional variation diagrams of magnetites and ilmenites from the ultra-alkaline Esquinzo complex (data are plotted in cations per formula unit).

All silicate rocks are clearly silica undersaturated and have normative nepheline. Nepheline syenitic rocks are the most undersaturated among the studied rocks. The pyroxenites of Tebeto and Las Montañetas, some perovskite-bearing ijolites from Barranco del Agua Salada, the biotitic malignites of Playa del Aguila, the pegmatitic ijolites from Las Montañetas and a nepheline syenite of Las Montañetas also have normative larnite as a consequence of their abundant modal calcite.

Pyroxenites, ijolites and nephelinites have low agpaitic indices (always lower than 1) and can be considered as subalkaline [88]. All Esquinzo nepheline syenites are chemically intermediate between agpaitic and miaskitic syenites [33]. Los Jablitos nepheline syenites have agpaitic indices between 0.8 and 1.3 and have normative acmite (2–13 wt%). Las Montañetas nepheline syenites from nepheline syenite–carbonatite composite dykes have

no normative acmite but their agpaitic indices also vary between 0.8 and 1.3. However, the abundance of biotite, titanite, apatite and zircon in these rocks indicates a miaskitic character. In Los Jablitos nepheline syenite, the agpaitic texture and zoned distribution of aegirine augite microlites indicate an agpaitic character. These mixed features are typical of intermediate nepheline syenites as previously indicated by [33].

All analyzed carbonatites have SiO_2 contents lower than 20 wt%, so they can be considered as carbonatites s.s (rocks are classified as carbonatites because more than 50 percent modal primary carbonates are present). They are classified as calciocarbonatites in the CaO-MgO-FeO diagram from [83] (Figure S13).

Figure S14 shows variation diagrams of MgO contents versus other elements. The highest MgO values are observed in perovskite-bearing amphibole pyroxenites (Las Montañetas) and perovskite-bearing pyroxenites (Playa de Esquinzo), while the lowest values occur in nepheline syenites (Jablitos and Las Montañetas). Intermediate values can be found in perovskite-bearing ijolites from Agua Salada Facies, feldspathic ijolites and malignites, pegmatite ijolites from Las Montañetas and nephelinites. In the silicate rocks, as MgO contents decreases, increases of SiO_2 , Al_2O_3 , K_2O , Na_2O , Rb and Ba and decreases of TiO_2 , Fe_2O_3 , CaO, P_2O_5 , Y, Nb, Ni, V, Ta, Co, Sc, U and REE can be observed. Zr and Hf show first an increase from pyroxenites to nepheline syenites (Jablitos and Las Montañetas), but later, a decrease in Los Jablitos nepheline syenite appears. Sr shows a general enrichment although some nepheline syenites (Las Montañetas and Los Jablitos) have a very low content.

High TiO_2 , P_2O_5 , Y, Sr, Nb, Ta, U and REE contents in perovskite-bearing amphibole pyroxenite of Las Montañetas facies (sample E-03-23, Table S13) compared to similar pyroxenites (see samples E-03-24 and E-03-9, Table S13) may be due to the higher abundances of perovskite and apatite in this rock. These rocks are cumulates.

Nepheline syenite E-03-19 (nepheline syenite–carbonatite composite dykes from Las Montañetas) commonly falls off the trends defined by the other rocks. It is characterized by high Sr, Ba, Y, Zr, Th, Hf, U and REE contents due to high abundances of alkali feldspar, calcite and zircon.

The observed elemental variations may be explained by fractional crystallization and/or accumulation of pyroxene, phlogopite, amphibole, apatite, titanite, magnetite and perovskite, and zircon at a late stage. Consequently, the pyroxenites can be considered as cumulates of pyroxene + apatite + magnetite + perovskite \pm amphibole \pm phlogopite. The proportion of these minerals determines the whole-rock composition of the pyroxenites. Carbonatites, in relation to associated silicate rocks, are strongly enriched in CaO, Sr, Y and REE, but are generally more depleted in all other elements.

All analyzed silicate rocks show quite steep REE patterns (Figure S15) with La/Yb(n) between 271 and 0.65. A gradual decrease in REE contents occurs from Las Montañetas perovskite-bearing amphibole pyroxenites to Los Jablitos nepheline syenites. Agua Salada medium-grained perovskite-bearing ijolites, Playa del Aguila feldspathic ijolites, Las Montañetas pegmatite ijolites/nepheline syenites and nephelinites have intermediate contents between those rocks. Nephelinite REE patterns are very similar to those presented by [25] for the nephelinite and phonolitic nephelinite fragments found in the oldest Formation of the S. V. G. (Basalts and Nephelinites from Barranco del Tarajalito). This gradual decrease in REE contents is accompanied by a decrease in La/Yb(n) ratio. Perovskite-bearing pyroxenites from Playa de Esquinzo have low REE values.

Jablitos nepheline syenites show concave REE patterns (Figure S15). The authors of [89] showed similar concave patterns and interpreted them as due to titanite fractionation and to zircon and melanite accumulation. Concentration of these minerals would produce high HREE compared to MREE contents. Moreover, titanite fractionation would produce a MREE decrease as this mineral concentrates MREE [90]. Similar concave patterns are common in nepheline syenites from the Khibiny and Lovozero plutons in Kola Alkaline province [91] or in nepheline syenites from Spitskop Complex, South Africa [92], and they have been explained by titanite fractionation [91]. Sample 7721 corresponds to a melanite-

bearing ijolite pegmatite showing a flat pattern characterized by HREE enrichment due to the presence of garnet. Nephelinites show quite fractionated patterns with almost flat HREE pattern, probably due to the common presence of titanite and garnet in these rocks.

Carbonatites have high REE contents and highly fractionated patterns with strong and steady increase in enrichment from Lu to La (Figure S15), resulting in very high La/Yb(n) values (9.54–56.05). Sample E-03-20 has a distinct REE pattern compared to other carbonatites. It shows a concave spectrum with strong HREE enrichment due to high zircon content. These features are typical for sövites genetically associated with nephelinites (A1 and A2 types after [93]). These sövites are also characterized by MgO-poor (<0.5 wt%), Sr-rich (>0.8 wt%) calcites and Si- and REE-rich apatites.

Figure S16 shows C1 chondrite-normalized spidergrams (chondrite values after [94]). All the rocks are enriched relative to chondrite composition. Pyroxenites, melteigites, ijolites and feldspathic ijolites show strong negative anomalies of Rb, K, P, Hf, Yb and Lu. Perovskite-bearing pyroxenites and ijolites show positive anomalies of U, Th, Ta, Nd and Eu, because of the occurrence of cumulate perovskite. Other pyroxenites, ijolites without perovskite and feldspathic ijolites lack Th- and U-positive anomalies but preserve Ta, Nd and Eu anomalies and show Ba and Ce anomalies. Nephelinites have negative anomalies of Rb, Th, K, P, Sm, Ti and Yb and positive anomalies of Ba, U, Nb, La, Sr, Nd and Zr.

Pegmatite ijolites show strong negative anomalies of Rb, K, P, Ti and Lu and positive anomalies of Th, Nb, Nd and Eu. Nepheline syenites show important negative anomalies in Rb, Ta, P, Sm and Ti and positive anomalies of Ba, Nb, Zr, Hf and Lu, indicating the presence of alkali feldspar, zircon, pyrochlore and the scarcity of titanite, apatite and ferromagnesian minerals in these rocks.

Esquinzo carbonatites show strong depletions in Rb, K, Ta, Ce, P, Zr, Hf and Ti and enrichment in La, Sr, Nd and Eu relative to chondrite C1. Zircon-bearing carbonatites show positive Zr and Hf anomalies. These patterns are comparable with average values of sövites [83].

Broadly speaking, in the rocks studied, the modal compositions coincide with the proportions obtained according to the CIPW standard. Figure 11 shows the normative compositions of the silicate studied rocks and phase relations in the system diopside-nepheline-sanidine at variable temperature at 0.1 GPa in the presence of water, where the cumulate nature of pyroxenites, melteigites, some ijolites and some pegmatite ijolites is pointed out. This diagram explains the crystallization trends followed by magmas involved in the generation of these rocks [95,96]. We can consider a melanephelinite as the initial melt (point X (Di₇₀ Ne₂₅ San₅), red circle in Figure 11). Melanephelinite is a melanocratic nephelinite with a higher concentration of pyroxene compared to nepheline. Figure 11 shows that diopside, within the simplified system whatever, should precipitate first from such a liquid. As the temperature drops, the liquid composition will move along diopside—X to 'a'. At point 'a', forsterite will co-precipitate with diopside, and the composition of the liquid should leave the diopside–nepheline–sanidine plane and move toward the diopside+nepheline+forsterite+liquid univariant (olivine nephelinite). Forsterite starts to react with the liquid and disappears around 985 ± 5 °C [95,96]. When the univariant line moves to point G and forsterite completely reacts out, the liquid comes back to the diopside–nepheline–sanidine plane. This could explain the absence of olivine in the studied rocks.

Nevertheless, if the nephelinite magma were sanidine-enriched (point Y, blue circle in Figure 11), the crystallization trend would not touch the diopside + nepheline + forsterite + liquid univariant line, and forsterite would not be formed. After the disappearance of forsterite, the liquid should move along the curve G–H with coprecipitation of nepheline and diopside resulting in the generation of a nephelinite. At H (865 °C), diopside, nepheline and leucite (nepheline leucitite) are in equilibrium with the liquid (Figure 11). Leucite starts to react with the liquid below 840 °C, and sanidine starts to appear (data from [96]). The assemblage at 840 °C, therefore, corresponds to a leucite and pyroxene-bearing phonolite (Le + Ne + San + pyroxene + L). Pargasitic amphibole precipitates just before the solidus

is reached (data from [96]), and the assemblage at 820 ± 10 °C corresponds to a potassic pargasite-bearing leucite–phonolite. Although the disappearance of leucite is not shown in this diagram, leucite is completely eliminated at 815 ± 10 °C (data from [96]), and the assemblage corresponds to a potassic pargasite-bearing phonolite.

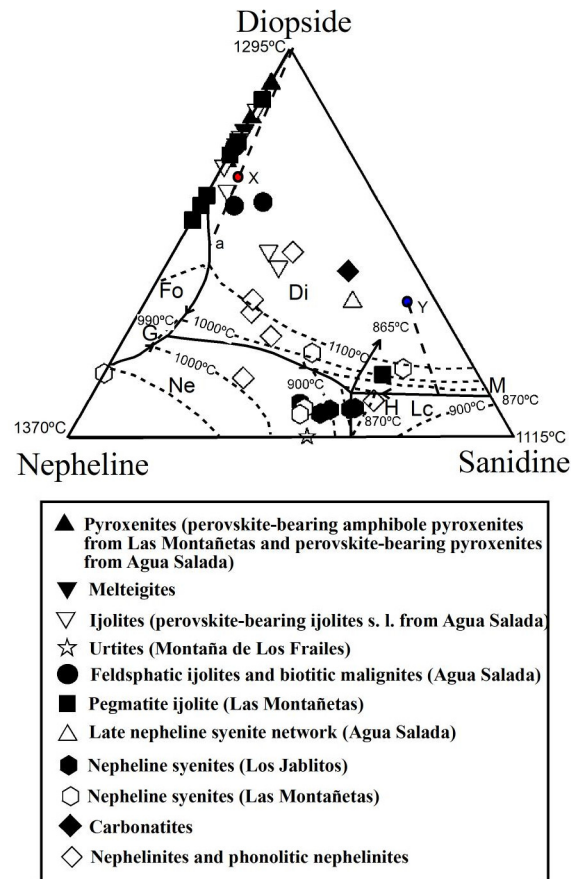


Figure 11. Normative compositions of the silicate studied rocks and phase relations in the system diopside–nepheline–sanidine at variable temperature at 0.1 GPa in the presence of water (after [95,96]).

In Figure 11, nepheline syenites plot near the equilibrium point at 815 °C where diopside, nepheline and sanidine and the latest residual melt coexist (data from [96]). This confirms the characterization of these rocks being the latest differentiates. On the other hand, only nephelinites and some nepheline syenites from Las Montañetas lie close to the curve G–H that marks melt evolution in equilibrium with nepheline and diopside. Consequently, these rocks can be considered as produced by melts rather than being magmatic cumulates.

The composition of silicate- and carbonate-rich rocks from Esquinzo are plotted on the diagram on Figure 12 [11]. Silicate rocks plot within the silicate liquidus field for the system $\text{CaO}-(\text{MgO} + \text{FeO}^*)-(\text{Na}_2\text{O} + \text{K}_2\text{O})-(\text{SiO}_2 + \text{Al}_2\text{O}_3 + \text{TiO}_2)-\text{CO}_2$ and form a linear trend from pyroxenites to nepheline syenites. Although the position of the miscibility gap between silicate and carbonatitic melts depends on the alkalinity of the silicate melts [14], and we cannot know this alkalinity in the case of the formation of the Esquinzo ultra-alkaline complex (due to the absence of melt inclusion studies), all Esquinzo silicate rocks fall far away from the curve that indicates the miscibility gap between silicate and carbonatitic melts. This trend begins at calcic pyroxene and ends in the areas of alkali feldspar and nepheline. This line describes the differentiation trend by fractional crystallization of pyroxene, perovskite and, in smaller amounts, phlogopite and amphibole that would produce cumulates (pyroxenites) and residual melts (syenites). Nephelinites have an intermediate position between perovskite-bearing ijolites and pegmatite ijolites-syenites.

E-03-19 syenite plots outside the general with high CaO contents because of the presence of calcite.

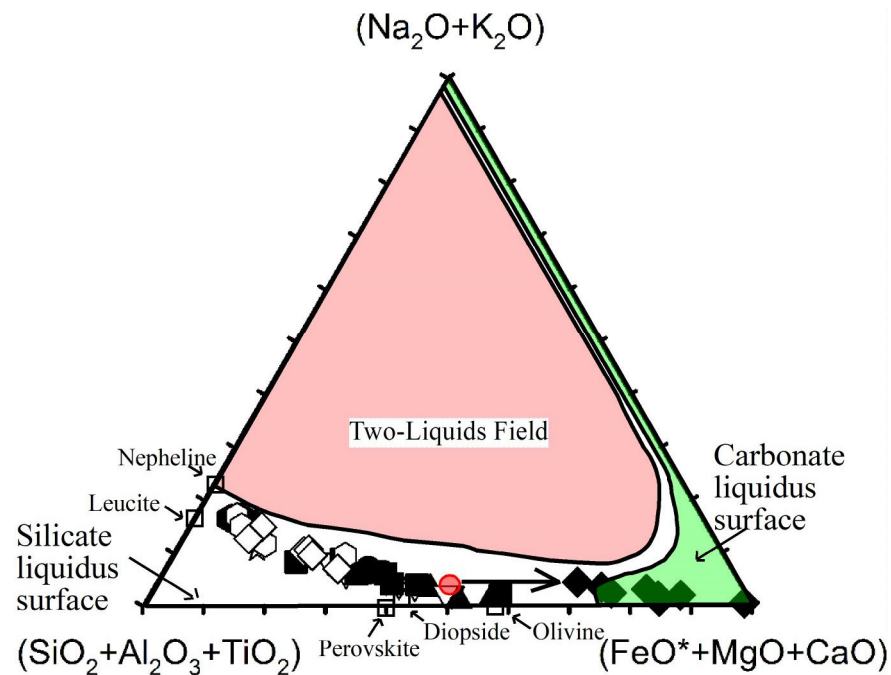


Figure 12. Composition of the studied rocks plotted on the “Hamilton projection” [12]. Possible residual path shown by bold continuous line with arrow (trend from more Si-rich, Ca-poor melteigites-ijolites toward the Si-poor, calcite-rich feldspathic ijolites that approach the silicate–carbonate liquidus field boundary). The 0.2 GPa phase field boundaries are from [11]. The fields defined in the diagram are for CaO-rich nephelinite from [12,14]. Symbols as in Figure 11. The red circle shows the position of the initial hypothetical melanephelinitic magma. FeO* is the total iron oxide expressed as FeO.

Some pegmatite ijolites (apatite-calcite pegmatite ijolites and feldspathic pegmatite ijolites) contain up to 20 modal % apatite and primary magmatic calcite. In Figure 12, these rocks show a continuous trend from more Si-rich, Ca-poor melteigites-ijolites toward the Si-poor, calcite-rich feldspathic ijolites that approach the silicate–carbonate liquidus field boundary. Precipitation of primary magmatic minerals (aegirine augite, biotite, nepheline, K-feldspar) was observed in these rocks and is consistent with the bulk-rock compositional trend on the Hamilton projection that supports fractional crystallization of a carbonated, hydrous nephelinitic magma toward a carbonatitic liquid.

In Figure 12, carbonatites plotted along a line from the calcite apex ($\text{FeO}^* + \text{MgO} + \text{CaO}$) to an area richer in alkalis and silica. This line marks the boundary between the carbonate and silicate liquidus surfaces. The position of the line away from the curves indicates the miscibility gap determined in numerous experimental works [9–12,97].

The occurrence of calcite and silicate minerals (pyroxene, titanite, nepheline and alkali feldspar) in equilibrium indicates simultaneous crystallization of these phases. This situation is only possible when the CO_2 -rich silicate melt reaches the composition marked by the boundary between the silicates and carbonates liquidus surfaces through differentiation. The authors of [11] demonstrated that fractional crystallization of a carbonate-rich melt with normative nepheline can arrive to a sequence of mineral associations similar to the one observed in the Oka complex (Canada) and also very similar to the Esquinzo ultra-alkaline complex (calcite and silicate minerals: pyroxene, titanite, nepheline and alkali feldspar). The authors of [98] explained, in a similar way, the origin of Dicker Willem carbonatitic complex (South Namibia) from a nephelinitic sövite magma.

4. Origin of the Different Rocks

4.1. Origin of Silicate Rocks

Field relations indicate the presence of at least three independent and consecutive magmatic pulses.

The first magma (of melanephelinite composition, indicated by the red circle in Figure 12) formed different silicate rocks by fractional crystallization of diopside, perovskite, apatite, magnetite, amphibole, phlogopite and nepheline. Crystallization probably took place in shallow magma chambers, where melts assimilated carbonates from the Mesozoic sediments of the oceanic crust, as shown by isotopic studies (C, O, H and S) on Fuerteventura carbonatites [99,100]. Differentiation of this magma by extreme local fractionation of pyroxene, nepheline, amphibole and phlogopite could produce a CO₂-rich silicate magma that formed the nepheline syenite–carbonatite composite dykes, silicocarbonatites and carbonatites of Las Montañetas and Montaña Los Frailes.

Relatively low Si activity during early crystallization of this magma is supported by the presence of perovskite and Ti-rich magnetite in the earliest formed cumulates. A subsequent increase of Si activity during the early stages of crystallization is shown by replacement of perovskite by titanite and of titanite by Ti-andradite in some pyroxenite, melteigites, ijolites and feldspathic ijolites. Anhedral perovskite is mantled by titanite, which, in turn, is mantled by Ti-andradite. The crystallizing sequence can be described as follows [67]:

$$\text{CaTiO}_3 \text{ (perovskite)} + \text{SiO}_2 \rightleftharpoons \text{CaTiSiO}_5 \text{ (titanite)}; \text{CaTiSiO}_5 \text{ (titanite)} + \text{SiO}_2 + \text{Fe}_2\text{O}_3 + 2\text{CaO} \rightleftharpoons \text{Ca}_3\text{Fe}_2\text{TiSi}_2\text{O}_{12} \text{ (Ti-andradite)}.$$

A continuous increase in Si activity with increased magma fractionation and/or a continuous decrease in the oxygen fugacity is indicated by the disappearance of perovskite (and titanomagnetite).

Malignites and feldspathic ijolites from Playa del Águila represent diopside pyroxene, biotite, apatite and perovskite cumulates that were impregnated by residual magma. Interstitial occurrence of alkali feldspar, nepheline and calcite together with the occurrence of augite and aegirine augite rims in diopside pyroxenes and mica zoning (from phlogopite to biotite) indicate the presence of this residual melt.

Two criteria allow a distinction to be made between the first and the second magmatic events. First, a field relationship was observed between feldspathic ijolites from the Barranco del Agua Salada, Los Jablitos nepheline syenites and late nepheline syenite network in Barranco del Agua Salada and Montaña de los Frailes Facies (second magmatic event) and the plutonic rocks of the early magmatic episode. Secondly, some minerals (e.g., pyroxene) show strong differences in their composition between the first and the second magmatic events (Figure 6). These two points indicate that feldspathic ijolites from Barranco del Agua Salada, Jablitos nepheline syenites and late nepheline syenite network in Barranco del Agua Salada and Montaña de los Frailes facies (second magmatic event) may, in fact, represent liquids produced by fractional crystallization of a distinct, younger parental nephelinite magma.

Extreme differentiation of this second magma batch via a similar mechanism to that acting on the early magma pulse could form the feldspathic ijolites from the Barranco del Agua Salada, Los Jablitos nepheline syenite and the late nepheline syenite network in Barranco del Agua Salada and Montaña Los Frailes Facies.

Finally, on the basis of field relations and geochemical compositions (mineral and whole rock), nephelinitic dykes again show a continuous trend toward the nephelinitic phonolite dykes, indicating the existence of a different nephelinite magma. The intrusive breccias with medium- to fine-grained ijolite-nephelinite matrix found in Barranco del Agua Salada Facies could also be related to the intrusion of this third magmatic pulse.

Thus, from a similar melanephelinite magma, two magmatic trends were obtained. In the early magmatic pulse, it evolved toward carbonatitic rocks, while the other two magmatic pulses differentiated toward a phonolitic/syenitic liquid.

None of the rocks found in the Esquinzo ultra-alkaline complex can represent the primary magma composition on the basis of low Mg/Mg+Fe ratios, low Ni and Cr contents of the rocks (Table S13) and textural features of magmatic cumulates present in many rocks. However, as indicated by their petrological characteristics, we can consider that the primary magma of the three magmatic pulses had a chemical composition close to a CO₂-rich melanephelinite. Fractional crystallization of the three magmatic pulses in shallow magma chambers produced the wide range of rocks found. This primary CO₂-rich melanephelinite melt probably originated by magmatic differentiation of an olivine nephelinite at the base of the crust.

The systematic occurrence of strong P- and K-negative anomalies in the C1-chondrite normalized spider diagrams (Figure S16) can be explained by the presence of residual apatite and phlogopite in the mantle source. Strong enrichment of LREE versus HREE suggests the presence of garnet in the residual mantle. Olivine nephelinite could be produced by the partial melting of a H₂O- and CO₂-rich mantle peridotite [101–104].

Figure S17 shows the conditions prevailing in Fuerteventura during the genesis of the Esquinzo ultra-alkaline complex. The age of the oceanic lithosphere at that time was approximately 140 Ma (note that the magmatism in this area began 30 Ma ago). Following [105], the thickness of the oceanic lithosphere increases with time up to an approximate age of 60 Ma, and it remains approximately constant from this time onward. Consequently, the thickness of an oceanic lithosphere of 140 Ma was equivalent to that of the lithosphere of around 60 Ma. The thickness of the oceanic lithosphere at the beginning of the volcanism in Fuerteventura has been estimated, in km, using the equations of [106,107]. In Figure S17, the geotherm calculated for oceanic lithosphere of around 140 Ma cuts the solidus for a H₂O-CO₂ peridotite at a depth of around 80 km, at the base of the lithosphere.

The genesis of the magmas of the Esquinzo ultra-alkaline complex of Fuerteventura may have consisted of the following steps (Figure 13 and Figure S17 with data from [108]):

1. The starting point is a thick (87–100 km) lithosphere around 140 Ma old with a Depleted Mantle (DM) composition, near the continental lithosphere with an EM (Enriched Mantle) signature [2].
2. The asthenosphere, either with an HIMU [2] or FOZO [109] signature, began to be particularly active during the Oligocene period in relation with a mantle plume or a large, thermally anomalous zone (after [110]).
3. In the upper zone of this anomaly or plume, which was volatile-rich and cooler than the inner zone, small-degree partial melting produced olivine melanephelinite magmas.
4. These melts may have assimilated part of the lithospheric mantle, which could have also contained EM elements, due to its proximity to the African continental lithosphere [2]. Also consider the involvement of a component of Subcontinental Lithospheric Mantle (SCLM) [111].
5. The melanephelinite melts ascended through the lithosphere, where olivine fractionation took place in deep chambers emplaced somewhere in the lithospheric mantle or at the base of the crust.
6. Melanephelinite melts reaching the crust began their stabilization, assimilation of carbonated sediments from the oceanic crust and differentiation at low pressures forming the Esquinzo ultra-alkaline complex and other equivalent complexes exposed in Fuerteventura (Ajuy-Solapa and Punta del Peñón Blanco).

The parental magmas that formed the various rocks in Esquinzo ultra-alkaline complex probably had similar features to olivine nephelinites formed at depths of more than 70 km, at the asthenosphere/lithosphere boundary or at the lithosphere base (Figure 13) by small degrees of partial melting of the head of a mantle plume or sublithosphere thermal anomaly (cooler and more volatile-rich than in its central part) in a pre-rift context without thermal erosion of the lithosphere. Oceanic crust at this moment was probably thickened by the contractive structures observed in the Submarine Volcanic Group and generated in a bulk compressive geodynamic setting [28].

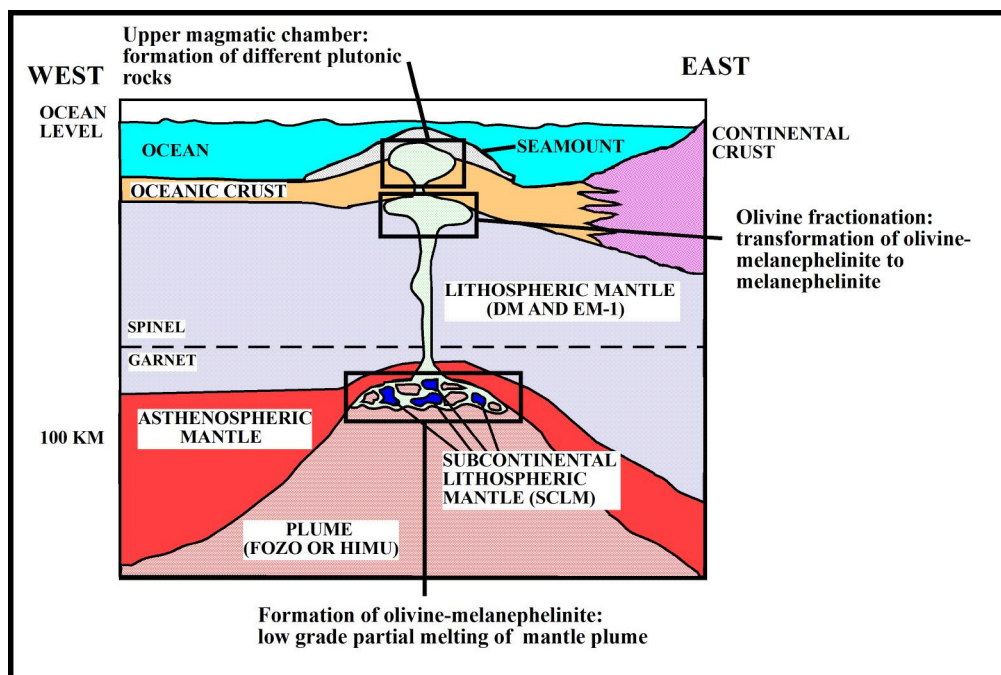


Figure 13. Model for the generation of the rocks of the Esquinzo ultra-alkaline complex. The spinel-garnet transition is located at 70–100 km [112,113].

4.2. Carbonatite Origin

As indicated in the introductory section, three main mechanisms [62] have been proposed to explain the origin of carbonatite rocks: (a) primary generation in the mantle [6,114]; (b) exsolution from a carbonated alkali-silicate melt via liquid immiscibility [115,116]; and (c) crystal fractionation of carbonated alkali silicate melts [16,117].

The authors of [3] favored the first mechanism to explain the origin of Fuerteventura carbonatites: primary generation in the mantle by melting of secondary calcitic carbonate in recycled carbonated oceanic crust (eclogite) with a recycling age of around 1.6 Ga. They recognized that in Fuerteventura, calcio-carbonatites are intimately associated with ijolite–nepheline syenite intrusive complexes and are cut by nephelinite–basanite through phonolite dikes and the associated silicate rocks have similar Sr–Nd–Pb isotopic compositions [2]. The authors of [3] discarded mechanism (b) because experimental data on the partitioning of trace elements between phonolite/carbonate and nephelinite/carbonate liquid pairs [118] are not consistent with an origin of the calcio-carbonatites from Fuerteventura through liquid immiscibility, assuming that the extremely high REE and very low Zr contents in the carbonatites to compare to the associated silicate rocks. Nevertheless, they did not consider the third mechanism proposed: crystal fractionation of carbonated alkali-silicate melts.

In the Esquinzo ultra-alkaline complex, there is distinct evidence that can explain the origin of carbonatites either by mechanism (b) or (c):

- (1) In Las Montañetas facies, there is a spatial-temporal relationship between carbonatites and silicate rocks, especially between ijolite pegmatites and nepheline syenite–carbonatite composite dykes, that indicates a strong genetic link between them. Pegmatite ijolites, nepheline syenites and carbonatites form commonly zoned dykes where carbonatites occupy the inner part. Although, in some outcrops, carbonatite veins cut nepheline syenite dykes, both rocks are coeval [18,33]. Sometimes carbonatites occur as bands and lenses within the syenites, and there are modal gradations between the two rock types, which may indicate that some of the carbonatites are also cumulates.

- (2) Although [3] considered some mineral phases in Fuerteventura carbonatites as xenocrysts (nepheline, aegirine augite or titanite), there is evidence that these minerals grew in equilibrium with calcite. Aegirine augite crystals in pegmatite ijolites, nepheline syenites, silicocarbonatites and carbonatites from Las Montañetas contain inclusions of calcite (Figure S5e), indicating their coprecipitation. Moreover, titanite crystals in carbonatites (Figure S4e) show idiomorphic habits and no sign of corrosion. Only in silicocarbonatites located near the wehrlite to gabbro Montaña Blanca intrusion [33], aegirine augite crystals show reaction coronas composed of magnetite, epidote, chlorite, titanite and calcite that can clearly be attributed to the thermal effect produced by the intrusion.

These textural features indicating equilibrium between calcite and silicate phases (aegirine augite, nepheline, titanite, etc.) in the silicocarbonatites from Las Montañetas and Montaña de Los Frailes contrast with disequilibrium textures observed by [119] in Alnö silicocarbonatites and by [120] in Prairie Lake complex silicocarbonatites, interpreted as the result of wallrock assimilation of silicate material by carbonatitic melts.

- (3) Calcite is ubiquitous as a late accessory mineral in all types of silicate rocks of the first magmatic event (pyroxenites, meltegités, ijolites and syenites). The chemical composition of those is very similar to the calcite crystals forming most of the carbonatite bodies (see Figure 9 and Table S8), which show high SrO concentration. These features are common to carbonatite calcites all over the world [121]. The authors of [12] demonstrated that calcite can be an igneous mineral formed by fractional crystallization of an evolved carbonated alkali-silicate melts. Thus, the common occurrence of calcite in the silicate rocks of the first magma batch can be explained by fractional crystallization of a very CO₂-rich silicate melt, related to carbonatite formation.
- (4) The similarity of composition of some minerals (diopside-hedenbergite-acmite proportions in pyroxenes, Fe/(Mg + Fe) versus Ti and Fe/(Mg + Fe) versus Al in biotites-phlogopites, Ba-K ratios in alkali feldspar, Figure 6, Figure 7 and Figure S6) present in some silicate rocks (nepheline syenites from the nepheline syenite-carbonatite composite dykes and ijolite pegmatites in Las Montañetas) and in carbonatites and silicocarbonatites. Clinopyroxenes show a continuous increase in Na and Fe_{TOT} (aegirine and hedenbergite components) and decrease in Ca (diopside component) with decreasing Mg (see Figure 6), which is consistent with normal closed system fractionation; it is similar to reported trends for other alkaline intrusions [64–67].
- (5) Isotopic compositions (Sr–Nd–Pb isotope data) of carbonatites are similar to those obtained for spatially related ijolites and nepheline syenites [2,3,109], suggesting a genetic relationship between the silicate and carbonate rocks. The authors of [2] explained the origin of Fuerteventura carbonatites by liquid immiscibility of a carbonated, alkaline silicate parent magma. Nevertheless, the position of these carbonatites and their associated silicate rocks far away from the liquid immiscibility curve [11,12,14] that consider carbonatite melts richer in alkalis and more depleted in CaO, in SiO₂ + Al₂O₃ + TiO₂-Na₂O + K₂O-MgO + FeOT + CaO diagram (Figure 13) excludes the origin of carbonatites by liquid immiscibility between a carbonatitic melt and a nephelinitic or syenitic melt.

Although some sövites are cumulates (those plotting near the corner of the FeO* + MgO + CaO in the diagram; in fact, calcite carbonatites cannot represent liquids [11]), their position in the Figure 13 is along the boundary of liquidus surfaces for carbonates and silicates. This is the unique situation when silicates and carbonates coprecipitate [11] and melts evolve to alkali- and SiO₂-rich and CaO-poor compositions. The existence of pegmatite ijolites and nepheline syenites with high contents of modal calcite (>10%) indicates that these rocks result from the crystallization of a carbonated melt along the boundary between the silicate-carbonate liquidus.

Moreover, Ta/Nb and Hf/Zr ratios are similar (Figure S18) in silicate rocks and carbonatites, thus excluding liquid immiscibility as a mechanism of carbonatite formation because the Nb-Ta and Zr-Hf element pairs are decoupled from each other, as Nb and, in

a lesser amount, Hf tend to be incorporated into the carbonatite melt, while Ta and Zr (a lower degree) partition in the silicate melt [13]. On the other hand, the high concentration of Zr and Hf in the nepheline syenites of Las Montañetas compared to the lower contents of these elements in the carbonatites is probably due to strong zircon fractionation in these syenitic magmas compared to their associated carbonatites.

Generating carbonatites by crystal fractionation of a carbonated silicate magma is an attractive hypothesis because the alkaline silicate rocks associated with carbonatites contain primary calcite. Primary magmatic calcite in alkaline silicate rocks is strong evidence for a fractionation path evolving toward a carbonate-rich, residual magma.

For all these reasons, we consider the following petrogenetic model to explain the origin of carbonatite at Esquinzo in a very similar way to that proposed by [122] for the Kovdor carbonatites.

Crystallization of the melanephelinite magma (which assimilated carbonated sediments from the oceanic crust) that produced the perovskite-bearing amphibole pyroxenites and pegmatite ijolites from Las Montañetas by accumulation of diopside, amphibole, perovskite, biotite and apatite, caused melt evolution that was characterized by increasing alkalis, CaO and volatiles (including CO₂) and decreasing SiO₂, following the trend shown in Figure 14.

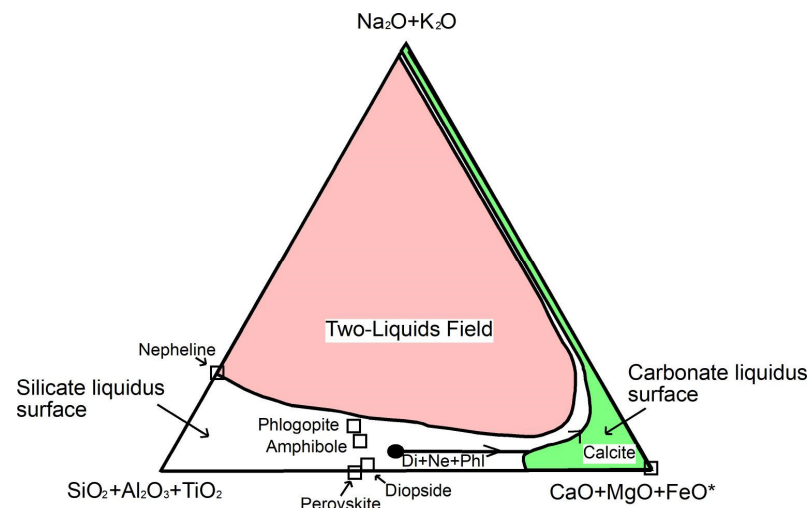


Figure 14. Hypothetical trend of the late-stage melt evolution in the studied rocks of Las Montañetas Facies present on the Hamilton projection. The 0.2 GPa phase field boundaries are from [11,12]. The circle denotes the position of the evolved larnite-normative melt; its further evolution is shown by arrows. Representative compositions of nepheline, diopside, perovskite, calcite and phlogopite-biotite mica are also shown. FeO* is the total iron oxide expressed as FeO.

The crystallization paths may not have intersected the two-liquid field but reached the calcite liquidus field in response to fractionation of the ne + cpx (+ phl + amph) assemblage. Fractionation continued along the silicate–carbonate field boundary toward the alkali-rich carbonatite eutectic. This is the trend proposed here for the ijolites to calcite carbonatites observed in Esquinzo. Continued fractionation resulted in the formation of clinopyroxene–nepheline-feldspar-calcite carbonatites. Liquidus phlogopite, and probably also amphibole, traversed thermal barriers between non-larnite-normative compositions of dry experimental systems (e.g., [123]). The stability and fractionation of liquidus phlogopite and amphibole thus led to an increase in CaO content of the liquid while the parental melanephelinite melts evolved to larnite-normative compositions, as suggested by [124] and shown experimentally by [125,126].

In conclusion, we can consider the following petrogenetic model to explain the formation of carbonatites at Esquinzo.

Fractional crystallization of amphibole, biotite, nepheline, pyroxene and perovskite from a nephelinite magma emplaced in the oceanic crust and simultaneous carbonate assimilation from these oceanic crustal blocks could form magmatic cumulates represented by pyroxenites and pegmatite ijolites from Las Montañetas, while the residual melt was progressively enriched in CaO, CO₂ and depleted in SiO₂, Al₂O₃, TiO₂, MgO and FeO up to the boundary between the silicate–carbonate liquidus curves.

At this point, formation of carbonatites began with coprecipitation of carbonates (calcite), silicates (aegirine augite, alkali feldspar, nepheline, biotite, titanite and zircon) and phosphates (apatite), to form nepheline syenite–carbonatite composite dykes and carbonatites.

Carbonatites are normally closely associated with alkaline volcanic rocks and intra-continental rifting (e.g., [127,128]). However, the carbonatites of the Canary and Cape Verde islands are associated with oceanic fracture zones [38,128]. In the Oman ophiolite, carbonatite occurrences are interpreted to be of primary mantle origin and to have formed in an oceanic island setting similar to the tectonic setting of the Canary and Cape Verde Islands [129,130]. These carbonatites are associated with large volumes of alkaline volcanic rocks, which were partly interpreted as within-plate magmas that erupted on volcanic islands or seamounts (e.g., [131]). These carbonatites and alkaline volcanics may have been generated during crustal thinning. This alkaline magmatic activity in Oman occurred largely during passive margin development, similar to the Canary and Cape Verde Islands.

In Fuerteventura, ultra-alkaline rocks seem to be associated with Miocene oceanic rifting considered by [28] as the tectonic result of the upwelling of a large body of anomalous asthenosphere, which exceeded the deformation associated with plate motions and generated a voluminous, tectonically controlled, basic volcanism during passive margin development.

Supplementary Materials: The following supporting information can be downloaded at: <https://www.mdpi.com/article/10.3390/min14030295/s1>, Figure S1: Simplified geological map of Fuerteventura modified from [29]; Figure S2: Relationships between the Oligocene and Miocene rock formation of Fuerteventura.; Figure S3: Relationships between the different lithologies of the Esquinzo ultra-alkaline Complex.; Figure S4: Microphotographs of the studied rocks; Figure S5: Microphotographs of the studied rocks; Figure S6: Composition variation diagrams of feldspars of the ultra-alkaline the Esquinzo Complex (data are plotted in cation per formula unit); Figure S7: Composition variation diagrams of nephelines from the ultra-alkaline the Esquinzo Complex (data are plotted in cation per formula unit); Figure S8: Composition variation diagrams of amphiboles from the ultra-alkaline Esquinzo Complex (data are plotted in cation per formula unit); Figure S9: Composition variation diagrams of titanites from the ultra-alkaline Esquinzo Complex (data are plotted in cation per formula unit); Figure S10: Composition variation diagrams of apatites from the ultra-alkaline Esquinzo Complex (data are plotted in cation per formula unit); Figure S11: Composition variation diagrams of perovskites from the ultra-alkaline Esquinzo Complex (data are plotted in cation per formula unit) and Chondrite CI-normalized REE patterns after [72] for perovskites; Figure S12: Composition variation diagrams of pyrochlores from the ultra-alkaline Esquinzo Complex (data are plotted in cation per formula unit) and Chondrite CI-normalized REE patterns after [72] for perovskites; Figure S13: Projection of Esquinzo carbonatite composition in the CaO-MgO-FeO diagram from [83]; Figure S14a,b: Composition diagrams (CaO, MnO, Fe₂O₃, Al₂O₃, TiO₂, SiO₂, P₂O₅, K₂O, Na₂O vs. MgOwt% in wt%; Ba, Sr, Rb, Ta, Hf, Zr, Y, Nb, Co, Ni, Sc, U, Th, V, REE vs. MgOwt% in ppm) comparing the whole-rock compositions of the studied rocks; Figure S15: REE distribution for whole rocks from selected samples normalized to the C1 chondrite of [94]; Figure S16: Element concentrations of the studied rocks normalized to the composition of C1 chondrite of [94]; Figure S17: Formation conditions of olivine melanephelinite that generated the studied rocks of Fuerteventura in the mantle; Figure S18: Zr-Hf and Ta-Nb (in ppm) distributions for the studied rocks; Text S1: The description of the methods used in the chemical analysis of the mineral phases and chemical analysis of selected rocks; Text S2: Petrographic description of the units; Text S3: Description of the chemical characteristics of amphiboles, titanites, apatites, perovskites and pyrochlores found in the Esquinzo ultra-alkaline complex; Table S1a–t: Representative analyses (in wt% of oxides) and formulae of pyroxenes from the Esquinzo ultra-alkaline rocks; Table S2a–m: Representative analyses (in wt% of oxides) and

formulae of micas from the Esquinzo ultra-alkaline rocks; Table S3a–II: Representative analyses (in wt% of oxides) and formulae of feldspars from the Esquinzo ultra-alkaline rocks; Table S4a,b: Representative analyses (in wt% of oxides) and formulae of nephelines from the Esquinzo ultra-alkaline rocks; Table S5a–c: Representative analyses (in wt% of oxides) and formulae of garnets from the Esquinzo ultra-alkaline rocks; Table S6a,b: Representative analyses (in wt% of oxides) and formulae of amphiboles from the Esquinzo ultra-alkaline rocks; Table S7a: Representative analyses (in wt% of oxides) and formulae of titanites from the Esquinzo ultra-alkaline rocks; Table S8a–e: Representative analyses (in wt% of oxides) and formulae of calcites from the Esquinzo ultra-alkaline rocks; Table S9a–e: Representative analyses (in wt% of oxides) and formulae of apatites from the Esquinzo ultra-alkaline rocks; Table S10a: Representative analyses (in wt% of oxides) and formulae of ilmenites from the Esquinzo ultra-alkaline rocks; Table S10b–i: Representative analyses (in wt% of oxides) and formulae of magnetites from the Esquinzo ultra-alkaline rocks; Table S11: Representative analyses (in wt% of oxides) and formulae of perovskites from the Esquinzo ultra-alkaline rocks; Table S12: Representative analyses (in wt% of oxides) and formulae of pyrochlores from the Esquinzo ultra-alkaline rocks; Table S13a–e: Rock analyses of the studied Fuerteventura rocks.

Author Contributions: Conceptualization: R.C., A.A., C.F. and A.D.; methodology: R.C., G.N. and A.D.; software: G.N. and A.D.; fieldwork and sampling: R.C. and A.A.; validation of results: R.C., A.A., C.F., A.D. and G.N.; formal analysis: G.N.; investigation: R.C., G.N. and A.D.; resources: R.C. and A.A.; data curation: R.C., G.N. and A.D.; writing—original draft preparation: R.C.; writing—review and editing: R.C., A.A., G.N., A.D. and C.F.; visualization: R.C. and G.N.; supervision: R.C., G.N. and A.D.; project administration: R.C. and A.D.; funding acquisition: R.C. and A.D. All authors have read and agreed to the published version of the manuscript.

Funding: This research was funded by projects CGL 2006-00970/BTE, CGL2009-07775, CGL2016-75062-P and PID2020-112920GB-I00 of the Spanish Ministry of Education, Science and the Spanish Ministry of Science and Innovation, Spanish Ministry of Science Innovation and Universities and Spanish Ministry of Science and Innovation; from project 2008/0250 (Agencia Canaria de Investigación, Innovación y Sociedad de la Información del Gobierno de Canarias); from an Integrated Action between Hungary and Spain (HH2004-0027 and MEC E-38/01, E-22/04); and the International Complementary Action PCI2006-A7-0520 of the Spanish Ministry of Education and Science is gratefully acknowledged.

Data Availability Statement: The authors confirm that the data supporting the findings of this study are available within the article and its Supplementary Materials.

Acknowledgments: We also thank the Cabildo Insular de Fuerteventura and the Spanish Ejército de Tierra (RIL Soria) for their help during the field work. We thank the four reviewers of this publication for the review work carried out and the correct suggestions issued.

Conflicts of Interest: The authors declare that there is no conflicts of interest.

References

1. Le Bas, M.J. Oceanic carbonatites. In *Kimberlites and Related Rocks*; Kornprobst, J., Ed.; Elsevier: Amsterdam, The Netherlands, 1984; pp. 169–178.
2. Hoernle, K.A.; Tilton, G.R. Sr–Nd–Pb isotope data for Fuerteventura (Canary Islands). *Schweiz. Mineral. Und Petrogr. Mitt.* **1991**, *71*, 3–18.
3. Hoernle, K.; Tilton, G.; Le Bas, M.J.; Duggen, S.; Garbe-Schönberg, D. Geochemistry of oceanic carbonatites compared with continental carbonatites: Mantle recycling of oceanic crustal carbonate. *Contrib. Mineral. Petrol.* **2002**, *142*, 520–542. [[CrossRef](#)]
4. Le Bas, M.J. Nephelinites and carbonatites. In *Alkaline Igneous Rocks*; Fitton, J.G., Upton, B.J.J., Eds.; Geological Society of London: London, UK, 1987; Special Publication 30; pp. 53–83.
5. Mitchell, R.H. Carbonatites and carbonatites and carbonatites. *Can. Mineral.* **2005**, *43*, 2049–2068. [[CrossRef](#)]
6. Wyllie, P.J.; Huang, W.L. Peridotite, kimberlite, and carbonatite explained in the system CaO–MgO–SiO₂–CO₂. *Geology* **1975**, *3*, 621–624. [[CrossRef](#)]
7. Wallace, M.E.; Green, D.H. An experimental determination of primary carbonatite magma composition. *Nature* **1988**, *335*, 343–346. [[CrossRef](#)]
8. Wyllie, P.J.; Lee, W.J. Model system controls on conditions for formation of magnesiocarbonatite and calciocarbonatite magmas from the mantle. *J. Pet.* **1998**, *39*, 1885–1893. [[CrossRef](#)]
9. Freestone, L.C.; Hamilton, D.L. The role of liquid immiscibility in the genesis of carbonatites—An experimental study. *Contrib. Mineral. Petrol.* **1980**, *73*, 105–117. [[CrossRef](#)]

10. Kjarsgaard, B.A.; Hamilton, D.L. Liquid immiscibility and the origin of alkali-poor carbonatites. *Mineral. Mag.* **1988**, *52*, 43–55. [[CrossRef](#)]
11. Lee, W.; Wyllie, P.J. Petrogenesis of carbonatite magmas from mantle to crust, constrained by the system CaO-(MgO + FeO*)-(Na₂O + K₂O) (SiO₂ + Al₂O₃ + TiO₂)-CO₂. *J. Petrol.* **1998**, *39*, 495–577. [[CrossRef](#)]
12. Kjarsgaard, B.A. Phase relations in a carbonated high-CaO nephelinite at 0.2 and 0.5 GPa. *J. Petrol.* **1998**, *39*, 2061–2075. [[CrossRef](#)]
13. Veksler, I.V.; Petibon, C.; Jenner, G.A.; Dorfman, A.M.; Dingwel, D.B. Trace element partitioning in immiscible silicate-carbonate liquid systems: An initial experimental study using a centrifuge autoclave. *J. Petrol.* **1998**, *39*, 2095–2104. [[CrossRef](#)]
14. Brooker, R.A.; Kjarsgaard, B.A. Silicate-Carbonate Liquid Immiscibility and Phase Relations in the System SiO₂-Na₂O-Al₂O₃-CaO-CO₂ at 0.1–2.5 G. Pa with Applications to Carbonatite Genesis. *J. Petrol.* **2010**, *52*, 1281–1305. [[CrossRef](#)]
15. Weidendorfer, D.; Schmidt, M.W.; Mattsson, H.B. Fractional crystallization of Si-undersaturated alkaline magmas leading to unmixing of carbonatites on Brava Island (Cape Verde) and a general model of carbonatite genesis in alkaline magma suites. *Contrib. Mineral. Pet.* **2016**, *171*, 43. [[CrossRef](#)]
16. Watkinson, D.H.; Wyllie, P.J. Experimental study of the join NaAlSiO₄-CaCO₃-H₂O and the genesis of alkalic rock-carbonatite complexes. *J. Petrol.* **1971**, *12*, 357–378. [[CrossRef](#)]
17. Lee, W.J.; Wyllie, P.J. Experimental data bearing on liquid immiscibility, crystal fractionation, and the origin of calcic carbonatites and natrocarbonatites. *Inter. Geol. Rev.* **1994**, *36*, 797–819. [[CrossRef](#)]
18. Fúster, J.M.; Cendrero, A.; Gastesi, P.; Ibarrola, E.; López Ruiz, J. *Geología y Volcanología de las Islas Canarias—Fuerteventura*; Instituto ‘Lucas Mallada’; Consejo Superior de Investigaciones Científicas: Madrid, Spain, 1968; pp. 1–239.
19. Stillman, C.J.; Fúster, J.M.; Bennell-Baker, M.J.; Muñoz, M.; Smewing, J.D.; Sagredo, J. Basal Complex of Fuerteventura (Canary Islands) is an oceanic intrusive complex with rift-system affinities. *Nature* **1975**, *257*, 469–471. [[CrossRef](#)]
20. Robertson, A.H.F.; Stillman, C.J. Late Mesozoic sedimentary rocks of Fuerteventura, Canary Islands. Implications for West Africa continental margin evolution. *J. Geol. Soc. Lond.* **1979**, *136*, 47–60. [[CrossRef](#)]
21. Robertson, A.H.F.; Stillman, C.J. Submarine volcanic and associated sedimentary rocks of the Fuerteventura Basal Complex, Canary Islands. *Geol. Mag.* **1979**, *116*, 203–214. [[CrossRef](#)]
22. Le Bas, M.J.; Rex, D.C.; Stillman, C.J. The early magmatic chronology of Fuerteventura. *Geol. Mag.* **1986**, *123*, 287–298. [[CrossRef](#)]
23. Stillman, C.J. A Canary Islands Dyke Swarm: Implications for the formation of oceanic islands by extensional fissural volcanism. In *Mafic Dyke Swarms*; Halls, H.C., Fahrig, W.J., Eds.; Geological Association of Canada Special paper 34, Geological Association of Canada: San Juan de Terranova, NL, Canada, 1987; pp. 243–255.
24. Steiner, C.; Hobson, A.; Favre, P.; Stampfli, G.M. Early Jurassic sea-floor spreading in the central Atlantic -the Jurassic sequence of Fuerteventura (Canary Islands). *Geol. Soc. Am. Bull.* **1998**, *110*, 1304–1317. [[CrossRef](#)]
25. Gutiérrez, M. Estudio Petrológico, Geoquímico y Estructural de la Serie Volcánica Submarina del Complejo Basal de Fuerteventura (Islas Canarias): Caracterización del Crecimiento Submarino y de la Emersión de la Isla. Ph.D. Thesis, Department of Pedology and Geology, Universidad de La Laguna, La Laguna, Spain, 2000; pp. 1–533.
26. Gutiérrez, M.; Casillas, R.; Fernández, C.; Balogh, K.; Ahijado, A.; Castillo, C. La serie volcánica submarina del Complejo Basal de Fuerteventura: Crecimiento submarino y emersión de la isla. *Geogaceta* **2002**, *32*, 250–254.
27. Gutiérrez, M.; Casillas, R.; Fernández, C.; Balogh, K.; Ahijado, A.; Castillo, C.; Colmenero, J.R.; García-Navarro, E. The submarine volcanic succession of the Basal Complex of Fuerteventura, Canary Islands: A model of submarine growth and emersion of some tectonic volcanic islands. *Geol. Soc. Am. Bull.* **2006**, *118*, 785–804. [[CrossRef](#)]
28. Fernández, C.; Casillas, R.; Navarro, E.; Gutiérrez, M.; Camacho, M.; Ahijado, A. Miocene rifting of Fuerteventura (Canary Islands). *Tectonics* **2006**, *5*, C6009. [[CrossRef](#)]
29. Balcells, R.J.; Barrera, J.L.; Gómez Sainz de Aja, J.A. *Mapa Geológico de España a Escala 1: 100:000*; Fuerteventura (92); Mapa y Memoria Instituto Geológico y Minero de España: Madrid, Spain, 2006; pp. 1–108.
30. Sagan, M.; Heaman, L.M.; Pearson, D.G.; Luo, Y.; Stern, R.A. Removal of continental lithosphere beneath the Canary archipelago revealed from a U—Pb Age and Hf/O isotope study of modern sand detrital zircons. *Lithos* **2020**, *362–363*, 105448. [[CrossRef](#)]
31. Casillas, R.C.; Fernández, C.; Colmenero, J.R. *Crecimiento Temprano y Evolución Geológica de la Isla de Fuerteventura*; 8th Meeting of the Iberian Group of Petrology, Geochemistry and Geochronology; Commission of Petrology, Geochemistry and Geochronology of Igneous and Metamorphic Rocks of the Spanish Geological Society: La Laguna, Spain; pp. 1–191.
32. Fúster, J.M.; Muñoz, M.; Sagredo, J.; Yébenes, A.; Bravo, T.; Hernández-Pacheco, A. Excursión nº 121 A + c del 26° I.G.C. a las Islas Canarias. *Boletín Inst. Geológico Y Min. España* **1980**, *92*, 351–390.
33. Barrera, J.L.; Fernández Santín, S.; Fúster, J.M.; Ibarrola, E. Ijolitas-Sienitas-Carbonatitas de los Macizos del Norte de Fuerteventura. *Boletín Inst. Geológico Y Min. España* **1981**, *92*, 309–321.
34. Cantagrel, J.M.; Fúster, J.M.; Pin, C.; Renaud, U.; Ibarrola, E. Age Miocène inférieur des carbonatites de Fuerteventura. *Comptes Rendus Acad. Sci. Paris* **1993**, *316*, 1147–1153.
35. Ahijado, A. Las Intrusiones Plutónicas e Hipoabisales del Sector meridional del Complejo Basal de Fuerteventura. Ph.D. Thesis, Department of Petrology and Geochemistry, Universidad Complutense de Madrid, Madrid, Spain, 1999; pp. 1–386.
36. Muñoz, M.; Sagredo, J.; De Ignacio, C.; Fernández-Santín, S.; Jeffries, T.E. New data (U-Pb, K-Ar) on the geochronology of the alkaline-carbonatitic association of Fuerteventura, Canary Islands, Spain. *Lithos* **2005**, *85*, 140–153. [[CrossRef](#)]
37. Casillas, R.; Ahijado, A.; Hernandez-Pacheco, A. Zonas de cizalla dúctil en el Complejo Basal de Fuerteventura. *Geogaceta* **1994**, *15*, 117–120.

38. Fernández, C.; Casillas, R.; Ahijado, A.; Perelló, V.; Hernández-Pacheco, A. Shear zones as result of intraplate tectonics in oceanic crust: An example of the Basal Complex of Fuerteventura (Canary Islands). *J. Struct. Geol.* **1997**, *19*, 41–57. [[CrossRef](#)]
39. Balogh, K.; Ahijado, A.; Casillas, R.; Fernández, C. Contributions to the chronology of the Basal Complex of Fuerteventura, Canary Islands. *J. Volcanol. Geotherm. Res.* **1999**, *90*, 81–102. [[CrossRef](#)]
40. Coello, J.; Cantagrel, J.M.; Hernán, F.; Fúster, J.M.; Ibarrola, E.; Ancochea, E.; Casquet, C.; Jamond, J.; Cendrero, A. Evolution of the eastern volcanic ridge of the Canary Islands based on new K-Ar data. *J. Volcanol. Geotherm. Res.* **1992**, *53*, 251–274. [[CrossRef](#)]
41. Ancochea, E.; Brandle, J.L.; Cubas, C.R.; Hernán, F.; Huertas, M.J. Volcanic complexes in the eastern ridge of the Canary Islands: The Miocene activity of the Island of Fuerteventura. *J. Volcanol. Geotherm. Res.* **1996**, *70*, 183–204. [[CrossRef](#)]
42. Muñoz, M. Estudio petrológico de las formaciones alcalinas de Fuerteventura (Islas Canarias). *Estud. Geológicos* **1969**, *25*, 257–310.
43. Hobson, A.; Bussy, F.; Hernández, J. Shallow-level migmatization of gabbros in a metamorphic contact aureole, Fuerteventura Basal Complex, Canary Islands. *J. Petrol.* **1998**, *39*, 125–137. [[CrossRef](#)]
44. Ahijado, A.; Casillas, R.; Hernandez-Pacheco, A. The dike swarms of the Amanay Massif, Fuerteventura, Canary Islands. *J. Asian Earth Sci.* **2001**, *19*, 333–345. [[CrossRef](#)]
45. Muñoz, M.; Sagredo, J. Reajustes mineralógicos y geoquímicos producidos durante el metamorfismo de contacto de diques basálticos (Fuerteventura, Islas Canarias). *Boletín Soc. Española Mineral.* **1994**, *17*, 86–87.
46. Muñoz, M.; Sagredo, J. *Existencia de Metamorfismos Superpuestos en el Complejo Basal de Fuerteventura (Canarias)*; I National Assembly of Geodesy and Geophysics: Madrid, Spain, 1975; pp. 1287–1288.
47. Muñoz, M.; Sagredo, J. Características del metamorfismo térmico producido por los eventos plutónicos intrusivos más recientes del Complejo Basal de Fuerteventura. In Proceedings of the ESF Meeting on Canarian Volcanism, Lanzarote, Spain, 30 November–7 December 1989; pp. 104–108.
48. Holloway, M.I.; Bussy, F.; Vennemann, T.W. Low-pressure, water-assisted anatexis of basic dykes in a contact metamorphic aureole, Fuerteventura (Canary Islands): Oxygen isotope evidence for a meteoric fluid origin. *Contrib. Mineral. Petrol.* **2007**, *155*, 111–121. [[CrossRef](#)]
49. Casillas, R.; Nagy, G.; Démeny, A.; Ahijado, A.; Fernández, C. Cuspidine-niocalite-baghdadite solid solutions in the metacarbonatites of the Basal Complex of Fuerteventura (Canary Islands). *Lithos* **2008**, *105*, 25–41. [[CrossRef](#)]
50. Casillas, R.; Démeny, A.; Nagy, G.; Ahijado, A.; Fernández, C. Metacarbonatites in the Basal Complex of Fuerteventura (Canary Islands). The role of fluid/rock interactions during contact metamorphism and anatexis. *Lithos* **2011**, *125*, 503–520. [[CrossRef](#)]
51. Meco, J.; Pomel, R.S. Les formations marines et continentales intervolcaniques des Iles Canaries Orientales (Grande Canarie, Fuerteventura et Lanzarote): Stratigraphie et signification paleoclimatique. *Estud. Geológicos* **1985**, *41*, 223–227. [[CrossRef](#)]
52. Cueto, L.A.; Balcells, R.; Barrera, J.L.; Gómez, J.A.; García, E.; Nieto, M.; Vidal, J.R.; Ruiz, M.T. *Mapa y Memoria Explicativa de la Hoja de Punta del Paso Chico (92-76) del Mapa Geológico Nacional*; Instituto Geológico y Minero de España: Madrid, Spain, 2004; scale 1:25,000, 1 sheet.
53. Cueto, L.A.; Balcells, R.; Barrera, J.L.; Gómez, J.A.; Vidal, J.R.; García, E.; Nieto, M.; Ruiz, M.T. *Mapa y Memoria Explicativa de la Hoja de la Oliva (93/94-76) del Mapa Geológico Nacional*; Instituto Geológico y Minero de España: Madrid, Spain, 2004; scale 1:25,000, 1 sheet.
54. Kamb, W.B. Ice petrofabric observations from Blue Glacier, Washington; in relation to theory and experiment. *J. Geophys. Res.* **1959**, *64*, 1891–1909. [[CrossRef](#)]
55. Demény, A.; Vennemann, T.W.; Hegner, E.; Ahijado, A.; Casillas, R.; Nagy, G.; Homonnay, Z.; Gutierrez, M.; Szabo, C. H, O, Sr, Nd, and Pb isotopic evidence for recycled oceanic crust in the Transitional Volcanic Group of Fuerteventura, Canary Islands, Spain. *Chem. Geol.* **2004**, *205*, 37–54. [[CrossRef](#)]
56. Mitchell, R.H. The melilitite clan. In *Undersaturated Alkaline Rocks: Mineralogy, Petrogenesis, and Economic Potential*; Mitchell, R.H., Ed.; Mineralogical Association Canada: Winnipeg, MB, Canada, 1996; Volume 24, pp. 123–152.
57. Le Bas, M.J. *Carbonatite—Nephelinite Volcanism*; J. Wiley and Sons: London, UK, 1997; pp. 1–347.
58. Woolley, A.R.; Kjarsgaard, B.A. Paragenetic types of carbonatite as indicated by the diversity and relative abundances of associated silicate rocks: Evidence from a global database. *Can. Mineral.* **2008**, *46*, 741–752. [[CrossRef](#)]
59. Zhabin, A.J. Primary textural-structural features of carbonatites and their metamorphic evolution. *Intern. Geol. Rev.* **1971**, *13*, 1087–1096. [[CrossRef](#)]
60. Cooper, A.F.; Reid, D.L. Textural evidence for calcite-carbonatite magmas, Dicker Willem, south-west Namibia. *Geology* **1991**, *19*, 1193–1196. [[CrossRef](#)]
61. Bowden, P.; Wall, F.; Schürmann, L. ‘Spinifex-textured’ pegmatitic crystallisation in carbonatites. *J. Afr. Earth Sci.* **2000**, *32*, A11–A12. [[CrossRef](#)]
62. Wyllie, P.J. Experimental studies of carbonatite problems. In *The Origin and Differentiation of Carbonatite Magmas, in: Carbonatites*; Tuttle, O.F., Gittins, J., Eds.; Wiley-Interscience: New York, NY, USA, 1966; pp. 311–352.
63. Morimoto, N.; Fabries, J.; Ferguson, J.; Ginzburg, I.V.; Ross, M.; Seifert, F.A.; Zussman, J.; Aoki, K.; Gottardi, G. Nomenclature of pyroxenes. *Am. Mineral.* **1988**, *73*, 1123–1133.
64. Nash, W.P. Mineralogy and Petrology of the Iron Hill carbonatite complex, Colorado. *Bull. Geol. Soc. Am.* **1972**, *83*, 361–382. [[CrossRef](#)]
65. Larsen, L.M. Clinopyroxene and coexisting mafic minerals from the alkaline Ilimaussaq intrusion, South Greenland. *J. Petrol.* **1976**, *17*, 258–290. [[CrossRef](#)]

66. Mitchell, R.H. Pyroxenes of the Fen alkaline complex, Norway. *Am. Miner.* **1980**, *65*, 45–54.
67. Vuorinen, J.H.; Hälenius, U.; Whitehouse, M.J.; Mansfelda, J.; Skelton, A.D.L. Compositional variations (major and trace elements) of clinopyroxene and Ti-andradite from pyroxenite, ijolite and nepheline syenite, Alno Island, Sweden. *Lithos* **2005**, *81*, 55–77. [[CrossRef](#)]
68. Marks, M.A.W.; Schilling, J.; Coulson, I.M.; Wenzel, T.; Markl, G. The alkaline-peralkaline Tamazeght complex, High Atlas Mountains, Morocco: Mineral chemistry and petrological constraints for derivation from a compositionally heterogeneous mantle source. *J. Petrol.* **2008**, *49*, 1097–1131. [[CrossRef](#)]
69. Le Bas, M.J.; Srivastava, R.K. Mineralogy and geochemistry of the Mundwara carbonatite dykes, Sirohi District, Rajasthan, India. *Neues Jahrb. Für Mineral.-Abh.* **1989**, *160*, 207–227.
70. McCormick, G.R.; Le Bas, M.J. Phlogopite crystallization in carbonatitic magmas from Uganda. *Can. Mineral.* **1996**, *34*, 469–478.
71. Hamilton, D.L. Nephelines as crystallization temperature indicators. *J. Geol.* **1961**, *69*, 321–329. [[CrossRef](#)]
72. McDonough, W.F.; Sun, S.S. The composition of the Earth. *Chem. Geol.* **1995**, *120*, 223–253. [[CrossRef](#)]
73. Deer, W.A.; Howie, R.A.; Zussman, J. Rock-forming minerals. In *Vol 1A Orthosilicates*, 2nd ed.; Longmans: London, UK, 1982; pp. 1–919.
74. Dawson, J.B.; Smith, J.V.; Steele, I.M. Petrology and mineral chemistry of plutonic igneous xenoliths from the carbonatite volcano, Oldoinyo-Lengai, Tanzania. *J. Petrol.* **1995**, *36*, 797–826. [[CrossRef](#)]
75. Huggins, F.E.; Virgo, D.; Huckenholz, H.G. Titanium-containing silicate garnets: II. The crystal chemistry of melanites and schorlornites. *Am. Mineral.* **1977**, *62*, 646–665.
76. Barros Gomes, C. Electron microprobe analysis of zoned melanites. *Am. Mineral.* **1969**, *54*, 1654–1661.
77. Vuorinen, J.H.; Halenius, U. Nb-, Zr- and LREE-rich titanite from the Alno alkaline complex: Crystal chemistry and its importance as a petrogenetic indicator. *Lithos* **2005**, *83*, 128–142. [[CrossRef](#)]
78. Flohr, M.I.K.; Ross, M. Alkaline igneous rocks of Magnet-Cove, Arkansas- metasomatized ijolite xenoliths from Diamond-Jo quarry. *Am. Mineral.* **1989**, *74*, 113–131.
79. Campbell, L.S.; Henderson, P.; Wall, F. Rare earth chemistry of perovskite group minerals from the Gardiner Complex, East Greenland. *Mineral. Mag.* **1997**, *61*, 197–212. [[CrossRef](#)]
80. Hogarth, D.D. Classification and nomenclature of pyrochlore group. *Am. Mineral.* **1977**, *62*, 403–410.
81. Atencio, D.; Andrade, M.B.; Christy, A.G.; Gieré, R.; Kartashov, P.M. The pyrochlore supergroup of minerals: Nomenclature. *Can. Mineral.* **2010**, *48*, 673–698. [[CrossRef](#)]
82. Möller, P. REE(Y), Nb and Ta enrichment in pegmatites and carbonatite alkalic rock complexes. In *Lanthanides, Tantalum and Niobium—Mineralogy, Geochemistry, Characteristics of Primary ore Deposits, Prospecting, Processing and Applications*; Möller, P., Cerny, P., Saupé, F., Eds.; Springer: New York, NY, USA, 1989; pp. 103–144.
83. Woolley, A.R.; Kempe, D.R.C. Carbonatites: Nomenclature, average chemical compositions and element distribution. In *Carbonatites: Genesis and Evolution*; Bell, K., Ed.; Unwin Hyman: London, UK, 1989; pp. 1–14.
84. Lumpkin, G.R.; Ewing, R.C. Geochemical alteration of pyrochlore group minerals: Microlite subgroup. *Am. Mineral.* **1992**, *77*, 179–188.
85. Lumpkin, G.R.; Ewing, R.C. Geochemical alteration of pyrochlore group minerals: Pyrochlore subgroup. *Am. Mineral.* **1995**, *80*, 732–743. [[CrossRef](#)]
86. Nasraoui, M.; Bilal, E. Pyrochlores from the Lueshe carbonatite complex (Democratic Republic of Congo): A geochemical record of different alteration stages. *J. Asian Earth Sci.* **2000**, *18*, 237–251. [[CrossRef](#)]
87. Hogarth, D.D. Pyrochlore, apatite and amphibole: Distinctive minerals in carbonatite. In *Carbonatites: Genesis and Evolution*; Bell, K., Ed.; Unwin Hyman: London, UK, 1989; pp. 105–148.
88. Sørensen, H. Alkali syenites, feldspathoidal syenites and related lavas. In *The Alkaline Rocks*; Sørensen, H., Ed.; John Wiley and Sons: London, UK, 1974; pp. 22–52.
89. De Ignacio, C.; Muñoz, M.; Sagredo, J.; Fernández-Santín, S. Mineralogía y geoquímica de las sienitas nefelínicas de Montaña Blanca-Esquinzo, NO de Fuerteventura (Islas Canarias). *Geotemas* **2004**, *6*, 29–32.
90. Eby, J.N.; Woolley, A.R.; Din, V.; Platt, G. Geochemistry and Petrogenesis of Nepheline Syenites: Kasungu-Chipala, Ilomba, and Ulindi Nepheline Syenite Intrusions, North Nyasa Alkaline Province, Malawi. *J. Petrol.* **1998**, *39*, 1405–1424. [[CrossRef](#)]
91. Downes, H.; Balaganskaya, E.; Beard, A.; Liferovich, R.; Demaiffe, D. Petrogenetic processes in the ultramafic, alkaline and carbonatitic magmatism in the Kola Alkaline Province: A review. *Lithos* **2005**, *85*, 48–75. [[CrossRef](#)]
92. Harmer, R.E. The petrogenetic association of carbonatite and alkaline magmatism: Constraints from the Spitskop complex, South Africa. *J. Petrol.* **1999**, *40*, 525–548. [[CrossRef](#)]
93. Horning-Kjarsgaard, I. Rare earth elements in sovitic carbonatites and their mineral phases. *J. Petrol.* **1998**, *39*, 2105–2121. [[CrossRef](#)]
94. Sun, S.S.; McDonough, W.F. *Chemical and Isotopic Systematics of OCEANIC Basalts*; Implications for Mantle Composition and Processes; Geological Society: London, UK, 1989; Volume 42, pp. 313–345. [[CrossRef](#)]
95. Chattopadhyay, S.; Chattopadhyay, B.; Gupta, A.K. Preliminary phase equilibria study of the system nepheline–diopside–sanidine under 1 kbar in presence of excess water. *Indian J. Geol.* **1999**, *71*, 81–91.

96. Gupta, A.K.; Chattopadhyay, S.; Chattopadhyay, B.; Arima, M. Experimental study of the system diopside–nepheline–sanidine at 1, 1 and 2 GPa [P(H₂O)=P(Total)]: Its significance in the genesis of alkali-rich basic and ultrabasic rocks. *Lithos* **2006**, *86*, 91–109. [[CrossRef](#)]
97. Kjarsgaard, B.A.; Hamilton, D.L. The genesis of carbonatites by immiscibility. In *Carbonatites: Genesis and Evolution*; Bell, K., Ed.; Unwin Hyman: London, UK, 1989; pp. 388–404.
98. Cooper, D.L.; Reid, D.L. Nepheline–sövites as parental magmas in carbonatite complexes: Evidence from Dicker Willem, southwest Namibia. *J. Petrol.* **1998**, *39*, 2123–2136. [[CrossRef](#)]
99. Demény, A.; Ahijado, A.; Casillas, R.; Boyce, A.J.; Fallick, A.E. Crustal contamination of carbonatites indicated by $\delta^{34}\text{S}$ – $\delta^{13}\text{C}$ correlations (Fuerteventura, Canary Islands). *Rev. Soc. Geológica España* **1998**, *12*, 453–460.
100. Demény, A.; Ahijado, A.; Casillas, R.; Vennemann, T.W. Crustal contamination and fluid/rock interaction in the carbonatites of Fuerteventura (Canary Islands, Spain): A C, O, H isotope study. *Lithos* **1998**, *44*, 101–115. [[CrossRef](#)]
101. Arculus, R.J. Melting behaviour of the two basanites in the range 10–35 Kbar and the effect of TiO₂ on the olivine–diopside reactions at high pressures. *Year Book—Carnegie Inst. Wash.* **1975**, *74*, 512–515.
102. Brey, G.P.; Green, D.H. Solubility of CO₂ in olivine melilitite at high pressures and role of CO₂ in the Earth’s upper mantle. *Contrib. Mineral. Petrol.* **1976**, *55*, 217–230. [[CrossRef](#)]
103. Brey, G.; Brice, W.R.; Elli, S.D.J.; Green, D.H.; Harris, K.L.; Ryabchikov, I.D. Pyroxene–carbonate reactions in the upper mantle. *Earth Planet. Sci. Lett.* **1983**, *62*, 63–74. [[CrossRef](#)]
104. Edgar, A.D. The genesis of alkaline magmas with emphasis on their source regions: Inferences for experimental studies. In *Alkaline Igneous Rocks*; Fitton, J.G., Upton, B.J.J., Eds.; Geological Society of London, Special Publication: London, UK, 1987; Volume 30, pp. 29–52.
105. Stein, C.A.; Stein, S. A model for global variation in oceanic depth and heat flow with lithospheric age. *Nature* **1992**, *359*, 123–129. [[CrossRef](#)]
106. Turcotte, D.I.; Schubert, G. *Geodynamics, Application of Continuum Physics to Geological Problems*; J. Wiley: New York, NY, USA, 1982; pp. 1–450.
107. Ranelli, G. *Rheology of the Earth*, 2nd ed.; Chapman and Hall: London, UK, 1995; pp. 1–413.
108. Wyllie, P.J. Origin of carbonatites: Evidence from phase equilibrium studies. In *Carbonatites: Genesis and Evolution*; Bell, K., Ed.; Unwin Hyman: London, UK, 1989; pp. 500–545.
109. De Ignacio, C.; Muñoz, M.; Sagredo, J.; Fernández-Santín, S.; Johansson, A. Isotope geochemistry and FOZO mantle component of the alkaline–carbonatitic association of Fuerteventura, Canary Islands, Spain. *Chem. Geol.* **2006**, *232*, 99–113. [[CrossRef](#)]
110. Hoernle, K.; Zhang, Y.S.; Schmincke, H.U. Seismic and geochemical evidence for large-scale mantle upwelling beneath the eastern Atlantic and western and central Europe. *Nature* **1995**, *374*, 34–39. [[CrossRef](#)]
111. Carnevale, G.; Caracausi, A.; Correale, A.; Italiano, L.; Rotolo, S.G. An Overview of the Geochemical Characteristics of Oceanic Carbonatites: New Insights from Fuerteventura Carbonatites (Canary Islands). *Minerals* **2021**, *11*, 203. [[CrossRef](#)]
112. Ito, K.; Kennedy, G.C. Melting and phase relations in the plane tholeiite–lherzolite–nepheline basanite to 40 kilobars with geological implications. *Contrib. Mineral. Petrol.* **1968**, *19*, 177–211. [[CrossRef](#)]
113. Bultitude, R.J.; Green, D.H. Experimental study of crystal–liquid relationships at high pressures in olivine nephelinite and basanite compositions. *J. Petrol.* **1971**, *12*, 121–147. [[CrossRef](#)]
114. Von Eckerman, H. The alkaline district of Alno Island. *Sver. Geoliska Unders.* **1948**, *36*, 176.
115. Von Eckerman, H. The petrogenesis of the Alno alkaline rocks. *Bull. Geol. Inst. Univ. Upps.* **1961**, *40*, 25–36.
116. Koster Van Groos, A.F.; Wyllie, P.J. Experimental data bearing on the role of liquid immiscibility in the genesis of carbonatites. *Nature* **1963**, *199*, 801–802. [[CrossRef](#)]
117. King, B.C. *The Napak Area of Southern Karamoja, Uganda*; Geological Survey Uganda: Kampala, Uganda, 1949; Mem 5; pp. 1–57.
118. Hamilton, D.L.; Bedson, P.; Esson, J. The behaviour of trace elements in the evolution of carbonatites. In *Carbonatites: Genesis and Evolution*; Bell, K., Ed.; Unwin Hyman: London, UK, 1989; pp. 405–427.
119. Vuorinen, H.; Skelton, A.D.L. Origin of silicate minerals in carbonatites from Alno Island, Sweden—Magmatic crystallisation or wall rock assimilation? *Terra Nova* **2004**, *16*, 210–215. [[CrossRef](#)]
120. Chakhmouradian, A.R.; Mitchell, R.H. *The Role of Assimilated Silica in the Evolution of Carbonatites*; 4th Eurocarb Workshop; Lanzarote–Fuerteventura: Canary Islands, Spain, 2003; pp. 10–11.
121. Kapustin, Y.U.L. *Mineralogy of Carbonatites*; Amerind Publishing Company Pvt., Ltd.: New Delhi, India, 1980; pp. 1–259, (translated from Mineralogiya Karbonatitov. Nauka Publ. Moscow, 1971).
122. Veksler, I.V.; Nielsen, T.F.D.; Sokolov, S.V. Mineralogy of Crystallized Melt Inclusions from Gardiner and Kovdor Ultramafic Alkaline Complexes: Implications for Carbonatite Genesis. *J. Petrol.* **1998**, *39*, 2015–2031. [[CrossRef](#)]
123. Yoder, H.S. Potassium-rich rocks: Phase analysis and heteromorphic relations. *J. Petrol.* **1986**, *27*, 1215–1228. [[CrossRef](#)]
124. Nielsen, T.F.D. Alkaline dike swarms of the Gardiner Complex and the origin of ultramafic alkaline complexes. *Geochem. Int.* **1995**, *31*, 37–56.
125. Fedorchuk, Y.A.M.; Veksler, I.V. Phase equilibria in the system akermanite–F–phlogopite at atmospheric pressure. *Geochem. Int.* **1997**, *35*, 197–199.

126. Veksler, I.V.; Fedorchuk, Y.A.M.; Nielsen, T.F.D. Phase equilibria in the silica-undersaturated part of the $\text{KAlSiO}_4\text{--Mg}_2\text{SiO}_4\text{--Ca}_2\text{SiO}_4\text{--SiO}_2\text{--F}$ system at 1 atm and the larnite-normative trend of melt evolution. *Contrib. Mineral. Petrol.* **1998**, *131*, 347–363. [[CrossRef](#)]
127. Le Bas, M.J. Ultra-alkaline magmatism with or without rifting. *Tectonophysics* **1987**, *143*, 75–84. [[CrossRef](#)]
128. Woolley, A.R. The spatial and temporal distribution of carbonatites. In *Carbonatites: Genesis and Evolution*; Bell, K., Ed.; Unwin Hyman: London, UK, 1989; pp. 15–37.
129. Nasir, S.; Klemm, R. New carbonatite occurrences along the Hatta transform fault zone (Northern Oman Mountains, United Arab Emirates). *J. Afr. Earth Sci.* **1998**, *27*, 3–10. [[CrossRef](#)]
130. Nasir, S.; Hanna, S.; Al-Hajari, S. The Petrogenetic Association of Carbonatite and Alkaline Magmatism: Constrains from the Masfut- Rawda Ridge, Northern Oman Mountains. *Mineral. Petrol.* **2003**, *77*, 235–258. [[CrossRef](#)]
131. Woolley, A.R.; Barr, M.W.C.; Din, V.K.; Jones, G.C.; Wall, F.; Williams, C.T. Extrusive carbonatites from the Uyaynah area, United Arab Emirates. *J. Petrol.* **1991**, *32*, 1143–1167. [[CrossRef](#)]

Disclaimer/Publisher’s Note: The statements, opinions and data contained in all publications are solely those of the individual author(s) and contributor(s) and not of MDPI and/or the editor(s). MDPI and/or the editor(s) disclaim responsibility for any injury to people or property resulting from any ideas, methods, instructions or products referred to in the content.